LA-UR-99-2353
Approved for public release; distribution is unlimited.

Title: **Strength Distributions and Size Effects for 2D and 3D Composites with Weibull Fibers in an Elastic Matrix**

Author(s): Sivasambu Mahesh, S. Leigh Phoenix, Irene J. Beyerlein

Submitted to:

Strength Distributions and Size Effects for 2D and 3D Composites with Weibull Fibers in an Elastic Matrix

Sivasambu Mahesh and S. Leigh Phoenix
Department of Theoretical and Applied Mechanics, Cornell University, Ithaca NY 14853.

Irene J. Beyerlein
Structure/Property Relations, Los Alamos National Laboratory, Los Alamos, NM 87545.

Abstract. Monte Carlo simulation and theoretical modeling are used to study the statistical failure modes in unidirectional composites consisting of elastic fibers in an elastic matrix. Both linear and hexagonal fiber arrays are considered, forming 2D and 3D composites, respectively. Failure is idealized using the chain-of-bundles model in terms of δ-bundles of length δ, which is the length-scale of fiber load transfer. Within each δ-bundle, fiber load redistribution is determined by local load-sharing models that approximate the in-plane fiber load redistribution from planar break clusters as predicted from 2D and 3D shear-lag models. As a result these models are 1D and 2D, respectively. Fiber elements have random strengths following either the Weibull or the power-law distribution with shape and scale parameters ρ and σ_δ, respectively. Simulations of δ-bundle failure, reveal two regimes. When fiber strength variability is low (roughly $\rho > 2$) the dominant failure mode is by growing clusters of fiber breaks up to instability. When this variability is high (roughly $0 < \rho < 1$) cluster formation is suppressed by a dispersed fiber failure mode. For these two cases, closed-form approximations to the strength distribution of a δ-bundle are developed under the local load-sharing model and an equal load-sharing model of Daniels, respectively. The results compare favorably with simulations on δ-bundles with up to 1500 fibers. The location of the transition in terms of ρ is affected by the upper tail properties of the fiber strength distribution as well as the number of fibers.

1. Introduction

Quasistatic failure of unidirectional composite materials, which consist of long aligned reinforcing fibers embedded in a matrix, is a complex random process. This complexity stems from the occurrence of various damage events preceding formation of a catastrophic crack, possibly including fiber breakage, matrix yielding, matrix cracking, fiber-matrix interfacial debonding, and fiber pull-out. Randomness, on the other hand, arises from variability in geometric, constitutive and fracture properties of the fibers, matrix and interface. Consequently the composite strength becomes a random quantity so that nominally identical specimens show statistical variation in their ultimate strengths.

Randomness in a constituent (fiber or matrix) property does not necessarily induce noticeable randomness in the corresponding composite property. For instance, global composite stiffness is fairly deterministic despite fluctuations in the local stiffness from material point to point as these fluctuations tend to average out over a sufficiently large volume. Composite strength, on the other hand, is largely determined by weak extremes of local strength (typically over the size scale of 5 to 100 fibers), which can lead to propagating material instabilities. Thus, local strength variability tends to persist through increasing size scale to cause strength variability at the global scale.

Analytical or numerical determination of the strength distribution of a composite structure, which reflects the full range of possible random micromechanical failure phenomena, is presently infeasible for realistic material volumes. Idealization of the local composite structure, constituent properties and stress redistribution mechanisms is therefore necessary. Sections 1.1–1.3 describe the idealizations made in this study followed by Section 1.4, which describes relevant literature.

1.1. Idealized composite structure and failure process

In idealizing the composite failure process we consider a composite consisting of a parallel array of n stiff, brittle, elastic fibers of cross sectional area A_{f} and length L, and embedded in a flexible, perfectly bonded, elastic matrix. Two arrays are considered: a linear array forming a 2D planar composite and a hexagonal array forming a 3D composite, as shown in Figure 1. We assume a high fiber-matrix stiffness ratio so that the fibers carry virtually all the tensile load. The composite is loaded by applying a far-field, tensile stress σ to the fibers so that total tensile load is approximately $n\sigma A_{\mathrm{f}}$. The matrix acts primarily to transfer load locally from broken to intact fibers through shear. This is idealized in terms of specific fiber load-sharing models in Section 1.2.

Variability is introduced by assuming that the fibers have random flaws distributed along them. In our main model these flaws follow Weibull-Poisson statistics. Thus, the strengths of individual fiber elements of small length δ are independent and identically distributed (i.i.d.) random variables that follow the Weibull distribution

$$F(\sigma) = 1 - \exp\left\{-\left(\sigma/\sigma_\delta\right)^\rho\right\}, \qquad \sigma \geq 0, \tag{1}$$

where $\rho \geq 0$ is the Weibull modulus or shape parameter and σ_δ is the Weibull scale parameter. Accordingly the mean strength of a fiber element is $\sigma_\delta \Gamma\left(1+1/\rho\right)$ and the coefficient of variation (standard deviation/mean) is $\sqrt{\Gamma\left(1+2/\rho\right)/\Gamma\left(1+1/\rho\right)^2 - 1}$. Except for very small ρ

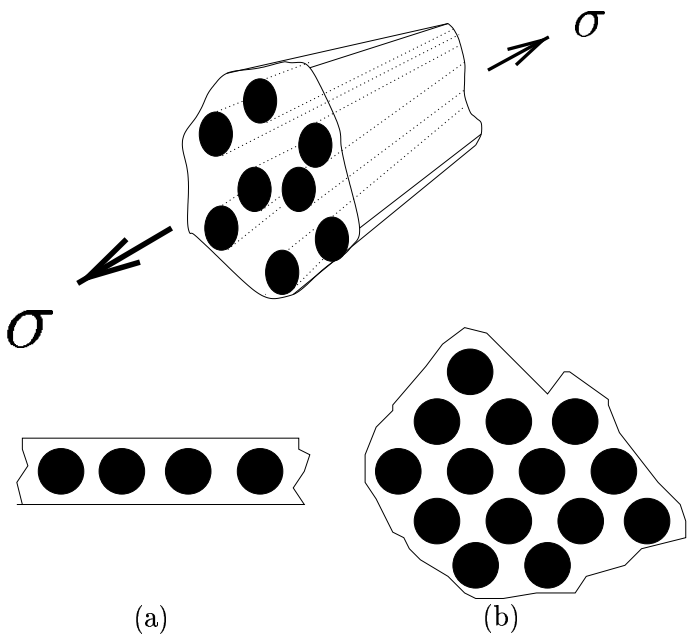

Figure 1. The two fiber arrays considered: (a) planar array and (b) hexagonal array. The far-field stress applied to the fibers is σ.

the mean differs very little from σ_δ. Note also that small ρ corresponds to large variability in fiber strength and vice versa.

By this model a length effect exists whereby σ_δ is related to the fiber strength at a convenient test gage length l_0 by $\sigma_\delta = \sigma_{l_0}(l_0/\delta)^{1/\rho}$ where σ_{l_0} is the Weibull scale parameter at l_0. Later we take δ to be a characteristic length of local fiber load transfer that depends on the geometric and material constitutive parameters in the shear-lag model. Thus σ_δ becomes a normalizing parameter for composite strength.

We also consider a variation on the Weibull distribution called the power-law distribution

$$F_p(\sigma) = \begin{cases} \left(\frac{\sigma}{\sigma_\delta}\right)^\rho & \text{if } 0 \le \sigma \le \sigma_\delta, \\ 1 & \text{if } \sigma_\delta < \sigma. \end{cases} \tag{2}$$

Clearly as $\sigma \downarrow 0$, $F(\sigma) \sim F_p(\sigma)$. Compared to the Weibull distribution Eq. (1), however, $F_p(\sigma)$ limits the maximum fiber strength to σ_δ. In this work we will compare results under Eq. (1) and Eq. (2) to understand the role that exceptionally strong fibers in the Weibull distribution play in δ-bundle failure, especially when ρ is small.

When a moderate tensile stress is applied to a composite specimen, fibers fail at random and the matrix surrounding each break serves to

transfer the lost fiber load to neighboring fibers through shear deformation. This stress transfer tends to occur over a certain length scale, δ, which is of the order of a few fiber diameters. The resulting local stress concentrations may cause neighboring fibers to fail without any further increase in the applied stress. In turn, these new breaks may cause even more breaks, and so on. After the formation of a certain number of breaks, many in small transverse clusters of various sizes, the system of fiber breaks may become stable. Then a small increment in applied stress will be needed to induce new breaks, which may create even more breaks due to increased stress concentrations. Eventually, after some stress increment, the system of fiber breaks becomes unstable and failure results from a cascade of breaks (possibly with cluster linking), which forms a wandering transverse crack.

As has been common in the literature, we idealize this failure process in terms of a longitudinal partition of $m = L/\delta$ transverse slabs or short bundles of length δ, called δ-bundles. The failure process within a given δ-bundle is treated as mechanically and statistically independent of that in neighboring δ-bundles. The composite is then treated as a weakest-link arrangement of these δ-bundles; that is, the composite fails when the weakest δ-bundle fails.

Modeling the failure process in a δ-bundle requires the strength statistics of its fibers of length δ as well as a model for redistribution of stress from broken to intact elements, which we refer to as the load-sharing model. This model should closely reflect the actual micromechanics of stress transfer around approximately transverse fiber break arrays in a realistic mechanical model of the composite irrespective of partitioning it into δ-bundles. Load-sharing models of varying degrees of idealization that we use are described next. (Henceforth the fiber elements within δ-bundles will be referred to as fibers.)

1.2. Fiber stress redistribution and load-sharing models

The simplest load-sharing model is the *equal load-sharing* (ELS) rule which we apply separately to each δ-bundle. Under ELS, if a δ-bundle has n fibers and j fibers have failed, the load concentration factor on each surviving fiber is $\kappa_{n,j} = n/(n-j)$, while all failed fibers carry no load. ELS is a reasonable assumption for a loose bundle of fibers (no matrix) clamped uniformly at each end. However, when the fibers are embedded in a matrix, the stress tends to concentrate on the intact fibers closest to the breaks. Thus ELS is not *a priori* an accurate mechanical description of stress redistribution at a composite cross-section. Nevertheless, theoretical results under ELS will turn out to be useful in interpreting dispersed fiber failure modes in a composite.

To account for the localized nature of fiber stress redistribution, *local load-sharing* (LLS) models have been devised, the simplest of which we call the *idealized local load-sharing* (ILLS) model. In a 2D planar composite, when fibers are broken within a given δ-bundle, a surviving fiber therein is assumed to have load concentration factor $K_r = 1 + r/2$ where r is the number of contiguous failed neighbors counting on both sides. In this 1D rule, a failed fiber shifts half of its load to the closest survivor on its left and half to the one on its right; more distant survivors receive no load. In a 3D unidirectional composite with fibers arranged in a hexagonal or square array, ILLS applied to a δ-bundle becomes 2D and load redistribution to nearest survivors requires additional assumptions on assigning portions based on the local configuration of failed fibers. For a large approximately round cluster where all the lost load is redistributed onto the ring of fibers around the circumference, $K_r = 1 + D/4$ where $r \approx \pi D^2/4$, and thus, D has units yielding one fiber per unit cross-sectional area. In reality, ILLS is too severe, i.e., the stress concentration on fibers immediately adjacent to a break cluster is lower than ILLS assumes, and the disparity increases with cluster size. Also, intact fibers more distant from the cluster experience some overloading due to longer range effects.

From a mechanics perspective, much more realistic load-sharing models for δ-bundles can be constructed from results based on shear-lag analysis of stress transfer around single transverse arrangements of fiber breaks in an infinite array of elastic fibers within an elastic matrix. Such models have been developed by Hedgepeth (1961) for 2D planar fiber arrays and by Hedgepeth and Van Dyke (1967) for 3D hexagonal or square fiber arrays. In these models the axial fiber and matrix shear stresses can be calculated at arbitrary locations in the composite. However, we only make use of the fiber stresses calculated along the transverse plane of the breaks, which reduces the resulting load-sharing to 1D and 2D, respectively. Fibers within a δ-bundle are treated as though the calculated fiber loads apply uniformly over their full lengths δ. By these restrictions, the fiber overloading is monotonic, i.e., the load in an intact fiber will be non-decreasing during the formation of new breaks. We refer to the 1D load-sharing model derived from the 2D case as *Hedgepeth local load-sharing* (HLLS) and the 2D model from the 3D case as *Hedgepeth and Van Dyke local load-sharing* (HVLLS).

In the Monte-Carlo simulations of δ-bundle failure we work with complete numerical versions of 1D HLLS and 2D HVLLS. The stresses are calculated numerically in every intact fiber for every arrangement of breaks that occurs in the simulations. Fundamental analytical solutions to the underlying shear-lag equations are coupled to a numerical weight-

ed superposition method to treat each configuration as for example in Beyerlein et al. (1996).

In developing probability models of the failure process, the above approach unfortunately results in serious analytical difficulties that require further idealizations to yield simpler rules for crucial configurations. In particular, only the stresses in intact neighbors adjacent to certain idealized, contiguous break clusters are defined. In HLLS a fiber next to an isolated group of r contiguous breaks is idealized as having load concentration factor $K_r = \sqrt{1+\pi r/4}$. In HVLLS the load concentration on the fibers around an approximately circular cluster of diameter D is approximated as $K_r = \sqrt{1+D/\pi}$ where again $r \approx \pi D^2/4$. The square-root feature in terms of cluster diameter indicates that these approximations are consistent with a continuum fracture mechanics viewpoint. Section 2 elaborates on their basis.

1.3. Composite strength distribution and Monte Carlo simulation approach

A key quantity of interest is the distribution function $G_n(\sigma)$ for δ-bundle strength. By the weakest link formula and chain-of-bundles assumption the strength of the composite of length $L = m\delta$ has distribution function $H_{m,n}(\sigma)$ given simply by

$$H_{m,n}(\sigma) = 1 - [1 - G_n(\sigma)]^m, \qquad \sigma \geq 0. \tag{3}$$

The key task is to determine $G_n(\sigma)$ in terms of $F(\sigma)$ for fiber strength and the load-sharing model for fibers in a δ-bundle.

In our model and Monte Carlo simulations we will assume periodic boundary conditions. Thus our 1D HLLS δ-bundles will form a tube, and under 2D HVLLS with hexagonal symmetry the simulation will be on a rhombus patch with doubly-periodic boundary conditions.

The Monte-Carlo algorithm for simulating failure is described in detail in Mahesh et al. (1999). In brief, to simulate the failure of a single δ-bundle, the first step is to assign numerical strength values to each fiber as sampled from the fiber strength distribution, Eq. (1) or Eq. (2). Then a load just sufficient to fail the weakest fiber is applied to the δ-bundle, and numerical stress redistribution is computed using either HLLS or HVLLS. If the new fiber stresses exceed the strengths of any other fibers then these too fail and stress redistribution for the new configuration is computed. This iterative process of fiber failures and stress redistribution is continued until either stability is reached or the δ-bundle fails catastrophically. If it becomes stable, a load increment is applied to the δ-bundle just sufficient to fail another fiber, and the above process is repeated. Eventually, at some load increment, a

cascade of fiber failures occurs as the δ-bundle fails. The applied fiber stress triggering the collapse is the strength of the δ-bundle.

The Monte-Carlo algorithm involves repeating the above procedure N $(= 500)$ times for each (n, ρ) pair, yielding N individual δ-bundle strengths. The empirical strength distribution $\hat{G}_n(\sigma)$ is constructed by plotting j/N against $\sigma_{(j)}$ for $j = 1, \ldots, N$ where $\sigma_{(j)}$ is the strength of the j^{th} weakest δ-bundle of the N simulated.

1.4. Results and insights from previous literature

Statistical modeling of the composite failure process has a long history. Pioneering work using the chain-of-bundles framework was carried out by Gücer and Gurland (1962), Rosen (1964) and Scop and Argon (1967), all using an ELS approach to δ-bundle failure based on work of Daniels (1945) and Coleman (1958). Zweben (1968), Scop and Argon (1969), Zweben and Rosen (1970), and Argon (1974) pursued LLS approaches to δ-bundle failure variously building on the works of Hedgepeth (1961) and Hedgepeth and Van Dyke (1967). These works not only initiated the discussion of dispersed versus localized cluster modes of fiber failure but also served to uncover the enormous difficulties in performing probability calculations. Harlow and Phoenix (1978a; 1978b; 1981), Smith (1980; 1983), Smith et al. (1983) and Phoenix and Smith (1983) simplified LLS to ILLS to capture the essence of localized fiber stress redistribution yet allow tractable analysis. Some of the large-ρ asymptotic results were also developed by Batdorf (1982) and Batdorf and Ghaffarian (1982) under relaxation of the chain-of-bundles and ILLS assumptions. This served to point out the robustness of the chain-of-bundles assumption as a means of capturing the crucial step of transverse evolution of failure clusters up to instability.

More rigorous analytical treatments for δ-bundles under 1D ILLS have also been carried out. See for example Kuo and Phoenix (1987), Harlow and Phoenix (1991), Leath and Duxbury (1994), and Zhang and Ding (1996). Other works such as those by Manders et al. (1982), Goda and Phoenix (1994), Beyerlein and Phoenix (1997a; 1997b) and Mahesh et al. (1999) have used Monte Carlo simulation interpreted by approximate probability calculations to treat δ-bundle failure under more realistic HLLS and HVLLS models. A full 3D failure simulation under a special version of HVLLS for square fiber arrays and avoiding the chain-of-bundles assumption was carried out by Landis et al. (2000). A lattice-based variation of HVLLS that also incorporated fiber slip and pullout during failure was developed by Ibnabdeljalil and Curtin (1997). An FEM-based, Monte Carlo model that also considered inter-

facial debonding was recently developed by Goda (1999). Overviews of relevant literature have been published by Curtin (1999) and Phoenix and Beyerlein (2000a).

The most important early work for ELS bundles (applied here to δ-bundles) was due to Daniels (1945) who showed that as the number of fibers n increases, the distribution for the strength of a bundle converges to a Gaussian or normal distribution with a fixed asymptotic mean, and a standard deviation that decreases as $1/\sqrt{n}$. As Smith (1982) and McCartney and Smith (1983) showed, the convergence of Daniels' Gaussian approximation to the true distribution is slow with an error approximately proportional to $n^{-1/6}$. By developing explicit corrections to the mean and variance that were proportional to $n^{-2/3}$, they obtained dramatic improvements to the Gaussian approximation that worked well even for bundles with as few as five Weibull fibers. These accurate results will form the basis for interpreting the dispersed fiber failure mode in our Monte Carlo simulations when ρ is small.

Harlow and Phoenix (1978a; 1978b) observed numerically that 1D ILLS δ-bundles with Weibull fibers obey weakest-link scaling beyond a certain size n. In particular, their strength distribution function, $G_n(\sigma)$ behaves such that $W_n(\sigma) = 1 - [1 - G_n(\sigma)]^{1/n}$ rapidly becomes independent of size n, converging as $n \to \infty$ to a characteristic distribution function $W(\sigma)$. This distribution embodied the key aspects of the localized statistical failure process. Phoenix and Smith (1983) gave a simple formula for constructing an accurate estimate of $W(\sigma)$ when fibers have modest to small strength variability (larger ρ). Beyerlein and Phoenix (1997a; 1997b) observed from Monte Carlo simulations that δ-bundles under a full implementation of 1D HLLS also show weakest-link behavior, and they developed an expression for $W(\sigma)$ that matched very well its empirical counterpart, $\hat{W}_n(\sigma)$.

1.5. Outline of the paper and main results

In the next section we describe the governing equations and main results for the shear-lag models for fiber breaks in planar and hexagonal arrays of fibers. The former forms the basis for 1D HLLS and the latter for 2D HVLLS used in Sections 3 and 4. Section 3 summarizes the Monte-Carlo simulation results using the framework in Mahesh et al. (1999), and makes connection between the dominant failure mode in a δ-bundle, i.e., cluster growth for large ρ and dispersed fiber failure for small ρ, and the behavior of its strength distribution. In Section 4, we study the cluster growth failure mode and derive results for the distribution function for composite strength in terms of a characteristic distribution function $W(\sigma)$ for which we develop closed-form approxi-

mations. We also develop results under the power-law distribution for fiber strength and through comparison to those under the Weibull case, as ρ decreases, we gain insight into the effects that a few extremely strong fibers can have on the results. We also develop expressions for the critical cluster size and size effect for composite strength. Section 5 focuses on the dispersed failure mode observed in the HVLLS and HLLS simulations for small ρ, and uses results on ELS δ-bundles to form tight lower bounds on the failure probabilities. Section 6 presents some analysis giving insight into the effects of ρ on probabilities and patterns of cluster growth. The final section draws connections to other work and summarizes insights achieved in the present work.

2. Load-Sharing Models for δ-Bundles

We now elaborate on the basis for the local load-sharing models used in the failure of δ-bundles, earlier referred to as HLLS and HVLLS. The description covers both numerical implementation and simplifications needed for analytical probability modeling.

2.1. Shear-lag model for a 2D planar fiber array: basis for HLLS

The shear-lag model for a 1D transverse array of breaks in a 2D planar fiber array was first studied by Hedgepeth (1961). In the model, fibers are assumed to deform in simple tension and the matrix deforms in simple shear. The fibers are loaded uniformly at $z = \pm\infty$ under tensile stress σ, where z is distance along the fiber direction away from the central transverse plane where breaks are located. We let $E_{\rm f}$ be the fiber tensile modulus, and $G_{\rm m}$ be the matrix shear modulus and assume $E_{\rm f} \gg G_{\rm m}$. Each fiber has cross sectional area $A_{\rm f}$, the effective matrix width between the fibers is w, the matrix thickness (perpendicular to the plane of the fibers) is h, the center-to-center fiber spacing is d and the fiber volume fraction is $V_{\rm f}$. A simple case is to assume h is also the main fiber cross-sectional dimension. Then $A_{\rm f} \approx h^2$, $d \approx w + h$, and $A_{\rm m} \approx wh$, where $A_{\rm m}$ is the cross sectional area of the matrix between two fibers. Thus the fiber volume fraction is $V_{\rm f} = A_{\rm f}/(A_{\rm f} + A_{\rm m}) \approx h/d$. Though exact for fibers of square cross section, these relations are useful approximations for circular fibers with radius $r_{\rm f} = h/2$. To simplify the discussion, all cross-sectional dimensions will be viewed as approximate, and our primary interest will be in the effects of fiber fractures at a length scale greater than the fiber diameter.

We ignore the part of the applied load carried by the matrix in tension, as well as matrix tension effects in the stress transfer process.

At the breaks we view the matrix as severed in the plane of the breaks and ignore any local singular-like stress concentrations in the fiber at a scale smaller than the fiber diameter. Many matrices locally yield rather than support such stresses. Unless $V_{\rm f}$ is small, ignoring matrix tension has little effect on stress transfer.

We let $\sigma_n(z)$ and $u_n(z)$ be the stress and displacement, respectively, in fiber n at location z along the fiber, where $-\infty < z < \infty$ and $n \in (\dots, -2, -1, 0, 1, \dots)$. In matrix bay n between fibers n and $n+1$, the effective shear force per unit length $q_n(z)$ is given by

$$q_n(z) = \frac{G_{\rm m} h}{w}(u_{n+1}(z) - u_n(z)). \tag{4}$$

The effective shear stress $\tau_n(z)$ and shear strain $\gamma_n(z)$ follow

$$\tau_n(z) = G_{\rm m}\gamma_n(z) = q_n(z)/h. \tag{5}$$

Hooke's law for the fiber gives

$$\sigma_n(z) = E_{\rm f}\frac{du_n(z)}{dz}, \tag{6}$$

and equilibrium of forces on a fiber element leads to

$$E_{\rm f}A_{\rm f}\frac{d^2u_n(z)}{dz^2} + \frac{G_{\rm m}h}{w}(u_{n+1}(z) - 2u_n(z) + u_{n-1}(z)) = 0. \tag{7}$$

The boundary conditions are $\sigma_n(z = \pm\infty) = \sigma$ for all fibers, $\sigma_n(0) = 0$ for the r fibers assumed to be broken on the $z = 0$ plane and $u_n(z) = 0$ for all intact fibers. We normalize the various quantities above using

$$\begin{aligned} P_n &= \sigma_n/\sigma, \\ U_n &= (u_n/\delta)(E_{\rm f}/\sigma), \\ T_n &= (h\delta/A_{\rm f})(\tau_n/\sigma), \\ \Gamma_n &= U_{n+1} - U_n = (\gamma_n G_{\rm m}/\sigma)(h\delta/A_{\rm f}), \\ \xi &= z/\delta, \end{aligned} \tag{8}$$

where δ is the length scale of load transfer given by

$$\delta = \sqrt{(E_{\rm f}A_{\rm f}w/(G_{\rm m}h)} = \sqrt{A_{\rm f}(E_{\rm f}/G_{\rm m})(w/h)}. \tag{9}$$

These normalizations yield a non-dimensional Hooke's law

$$P_n(\xi) = \frac{dU_n(\xi)}{d\xi}, \tag{10}$$

and a non-dimensional system of equations

$$\frac{d^2U_n(\xi)}{d\xi^2} + U_{n+1}(\xi) - 2U_n(\xi) + U_{n-1}(\xi) = 0, \tag{11}$$

with normalized boundary conditions

$$\begin{aligned} P_n(\pm\infty) &= 1, \quad -\infty < n < \infty \\ P_n(0) &= 0, \text{ on all } r \text{ broken fibers,} \\ U_n(0) &= 0, \text{ for all other fibers.} \end{aligned} \tag{12}$$

For a single break at $n = 0$ and $z = 0$ this set of equations can be solved for all z using discrete Fourier transform methods. This leads to influence functions for the effects of a single break on stress and displacements at all fiber and matrix locations. An arbitrary array of multiple breaks lying within a single plane can then be handled using a superposition of influence functions translated to the actual break locations and appropriately weighted to satisfy the boundary conditions. This operation requires numerically solving an $r \times r$ matrix equation where r is the number of breaks[1]. In the Monte Carlo simulations of δ-bundle failure, we use this method to numerically calculate the fiber loads for all break arrays that occur. A similar approach was used in Beyerlein et al. (1996) and Beyerlein and Phoenix (1997a; 1997b). This constitutes the 1D load-sharing model called HLLS.

In the probability analysis for HLLS under large ρ we use accurate approximations to the load concentrations due to an isolated cluster of r contiguous fiber breaks in a single plane, or r-cluster. Specifically we want the peak load concentration factor (at the $z = 0$ plane) on the nearest neighbor, denoted K_r. We also want the load concentration factor $K_{r,s}$ on fiber number s ahead of an r-cluster. Some results due to Hedgepeth (1961) and Hikami and Chou (1990) are reviewed in Beyerlein et al. (1996) and approximations were developed there using Stirling's formula. The approximations

$$K_r \approx \sqrt{\frac{\pi r}{4} + 1}, \tag{13}$$

and

$$K_{r,s} \approx K_r \sqrt{\frac{1}{\pi(s-1)+1}}, \tag{14}$$

[1] This method works for the more general problem in which the breaks do not lie within a single plane (Beyerlein et al., 1996). In that case numerical integration is required in evaluating the influence functions. In our case of aligned breaks the influence functions are simple expressions.

are minor improvements on theirs, which are extremely accurate even for small r. For larger clusters the latter result is only useful for s within about $r/4$ of the cluster edge, at which point the stress concentration reaches the far-field value, unity, as seen in Beyerlein et al. (1996). Note also that for the fiber subadjacent to the last break of a large r-cluster, the load concentration is about one-half the value on the adjacent fiber.

2.2. Shear-lag model for a 3D hexagonal fiber array: basis for HVLLS

In a 3D hexagonal array of fibers, as considered by Hedgepeth and Van Dyke (1967) and shown in Figure 1, similar ideas apply as in the previous section. The fibers are identified by the index pair, (m,n) corresponding to axes in the transverse plane with included angle $\pi/3$ radians. All displacement and stress quantities have subscript (m,n) to replace n in the planar case and the normalizations are the same. The main change relative to the planar fiber array is that the non-dimensional differential equation for the dimensional displacement $u_{(m,n)}$ of fiber (m,n) becomes

$$\frac{d^2U_{(m,n)}(\xi)}{d\xi^2} + \Big(U_{(m+1,n)}(\xi) + U_{(m,n+1)}(\xi) + U_{(m-1,n)}(\xi) + U_{(m+1,n-1)}(\xi) + U_{(m-1,n+1)}(\xi) - 6U_{(m,n)}(\xi)\Big) = 0. \tag{15}$$

Thus, six interfiber couplings exist for each fiber instead of two as in a planar array. The boundary conditions are similar to those given by Eq. (12) except the break array is 2D. The numerical implementation in calculating the fiber stresses is also similar. This constitutes the 2D load-sharing model called HVLLS.

In the probability analysis for HVLLS under large ρ we use accurate approximations to the load concentrations due to an isolated cluster of r contiguous fiber breaks in a single plane, or r-cluster. We focus on the stress concentrations around a penny-shaped r-cluster. First we define an effective fiber spacing d and a dimensionless diameter D of the penny. The effective fiber spacing is chosen so that there is one fiber per unit cross-sectional area. In a hexagonal array, one fiber and matrix unit occupies area $\sqrt{3}d'^2/2$ where d' is the center-to-center fiber spacing so that $d = (\sqrt[4]{3}/\sqrt{2})d' \approx 0.9306d'$. We define D such that $r = \pi D^2/4$ so that the effective cluster diameter is Dd. The fibers surrounding the r-cluster are subjected to the "effective" stress concentration

$$K_r \approx \sqrt{\frac{D}{\pi} + 1} = \sqrt{\frac{2\sqrt{r}}{\pi^{3/2}} + 1}. \tag{16}$$

For the decay of the stress concentration with distance we find

$$K_{r,s} \approx \frac{K_r}{\sqrt{\pi(s-1)+1}}, \tag{17}$$

is a reasonable approximation, where s is the number of effective fiber spacings d (not necessarily an integer) a fiber is away from an effective cluster radius $\bar{R} = (D-1)/2$. For larger D this result is only valid for s within about $D/10$ of the edge of the cluster, beyond which the stress concentration drops very close to the far-field value, unity. See Mahesh et al. (1999) and Phoenix and Beyerlein (2000a) for elaboration.

3. Failure Mechanisms in δ-bundles

We now describe certain qualitative trends observed in the Monte Carlo simulations of δ-bundle failure. The observed failure mechanisms appear to play a fundamental role in determining the behavior of the strength distribution. The cause and effect relationship seems clearest when viewed in terms of the variability in fiber strength through ρ.

3.1. Small variability in fiber strength (large ρ)

For $\rho = 10$, snapshots of the damage evolution *en route* to δ-bundle failure in median ($N = 500$) 2D and 3D specimens are shown in Figures 2 and 3, respectively, where the boundary conditions are periodic. In each figure, the last stage corresponds to the pattern of breaks immediately after the formation of an unstable configuration and before collapse. We separately label the first fibers to fail after the point of instability. Since the boundary conditions are periodic a break cluster appearing at one edge (side or top) may be continued on the opposite edge.

When ρ is large (low variability in fiber strength), the tendency to form break clusters and propagate them appears to be the dominant failure mode (Figures 2 and 3). As breaks form under increasing applied load, they overload their neighbors more intensely than more distant fibers. The probability of failure of a neighbor is thus enhanced since the neighboring fibers are unlikely to be much stronger than the broken fiber. This leads to the formation of a cluster of breaks, which in turn imparts even larger stress concentrations on its neighbors and the cluster therefore propagates with increasing probability as it grows. Eventually the cluster becomes unstable and fails the composite.

As mentioned, Harlow and Phoenix (1978b) observed that the strength distribution of a composite with a cluster-forming failure mode lends itself to weakest-link scaling analysis. They found that the cumulative

Figure 2. Snapshots of the failure process in median strength ($N = 50$) 1D δ-bundles with 30 Weibull fibers for $\rho = 10$ and periodic boundary conditions. ◯ intact fibers, ⊗ broken fibers and ⊙ first fibers to fail after instability.

distribution function for the strength of a δ-bundle under 1D ILLS has the form

$$G_n(\sigma) \approx 1 - [1 - W(\sigma)]^n, \qquad \sigma \geq 0, \tag{18}$$

when the bundle size n is larger than a certain critical size, where $W(\sigma)$ was earlier called the characteristic distribution function. The threshold for n turns out to be the critical cluster size $k(\sigma)$ for instability in the δ-bundle, being approximately defined by $K_k\sigma \approx \sigma_\delta$.

Using Weibull coordinates, we have plotted in Figure 4 the empirical weakest-link distributions

$$\hat{W}_n(\sigma) = 1 - [1 - \hat{G}_n(\sigma)]^{1/n}, \qquad \sigma \geq 0, \tag{19}$$

obtained from our Monte-Carlo failure simulations of the empirical distribution function for δ-bundle strength, $\hat{G}_n(\sigma)$, under 1D HLLS. For $\rho \geq 1$ the $\hat{W}_n(\sigma)$ curves for $n = 225$, 625 and 900 collapse onto one characteristic curve $\hat{W}(\sigma)$, but not for $\rho = 1/2$. The plotted results suggest that the cluster growth failure mode is active for $\rho \geq 1$. From the δ-bundle failure stresses observed in the simulations, rough estimates of the corresponding critical cluster sizes k are obtained from solving $K_k\sigma = \sigma_\delta$, using Eq. (13). In all cases k is at least an order of magnitude smaller than the size of the smallest bundle $n = 225$. For $\rho = 1$ it is less than 15 and is about 10 for $\rho = 3$. This suggests that Eq. (18) applies for the δ-bundle stress and size range shown, which is significant since it gives a size scaling for the strength distribution in terms of n. Figure 4 also shows a reversal in the weakening trend as ρ decreases from 10 to 1 to a strengthening trend as ρ decreases below 1. The latter is due to very strong fibers from the upper tail of the $\rho = 0.5$ Weibull distribution, which is examined further in Section 3.2.

For 2D δ-bundles under HVLLS, empirical weakest-link distributions $\hat{W}_n(\sigma)$ are shown in Figure 5, and a similar collapse to $\hat{W}(\sigma)$ is seen for

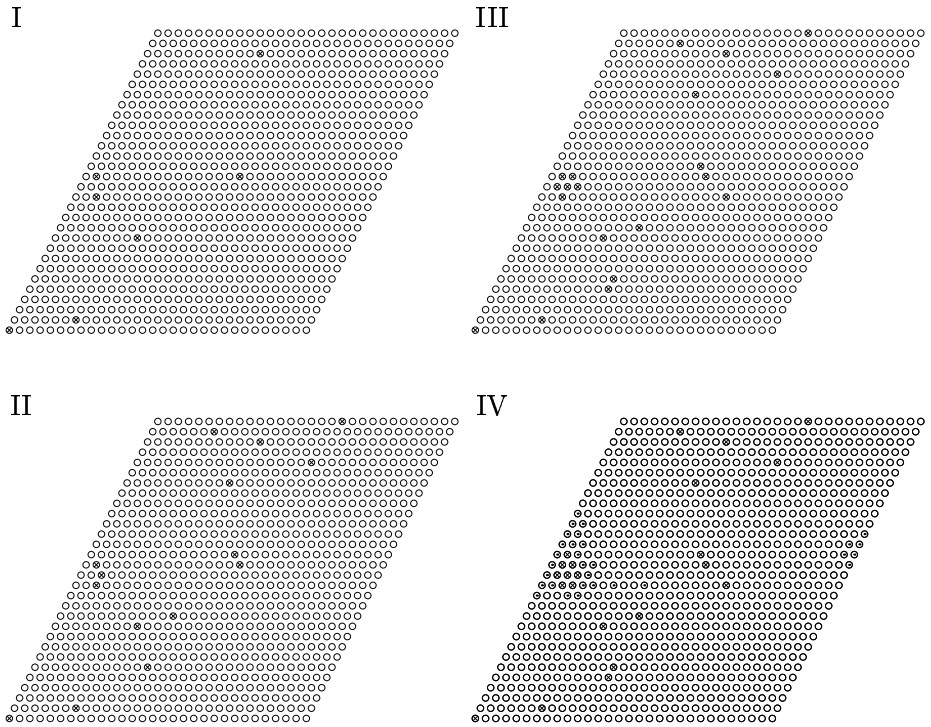

Figure 3. Snapshots of the failure process in median strength ($N = 500$) 2D δ-bundles with 900 Weibull fibers for $\rho = 10$ and periodic boundary conditions. ◯ intact fibers, ⊗ broken fibers, and ⊙ first fibers to fail after instability.

$\rho = 5$ and 10. For $\rho = 2$ and 3 the collapse is less sharp than in 1D, and it worsens rapidly as ρ is decreased further. For $0 < \rho \leq 2$, analysis of the critical cluster size k from solving $K_k\sigma = \sigma_\delta$, using Eq. (16), shows that k approaches the size of the smallest bundle. Thus the lack of collapse of the $\hat{W}_n(\sigma)$ curves to one master curve $\hat{W}(\sigma)$ does not necessarily imply that cluster growth dominated failure no longer dominates, an issue we revisit later.

For larger ρ, the strength distribution for δ-bundles under 2D HVLL-S is governed by the lower tail of the fiber strength distribution, as is seen by considering two modified Weibull distributions,

$$\overline{F}(\sigma) = \begin{cases} F(\sigma) & \text{if } 0 \leq \sigma < \sigma_\delta, \\ 1 & \text{if } \sigma_\delta \leq \sigma, \end{cases} \tag{20}$$

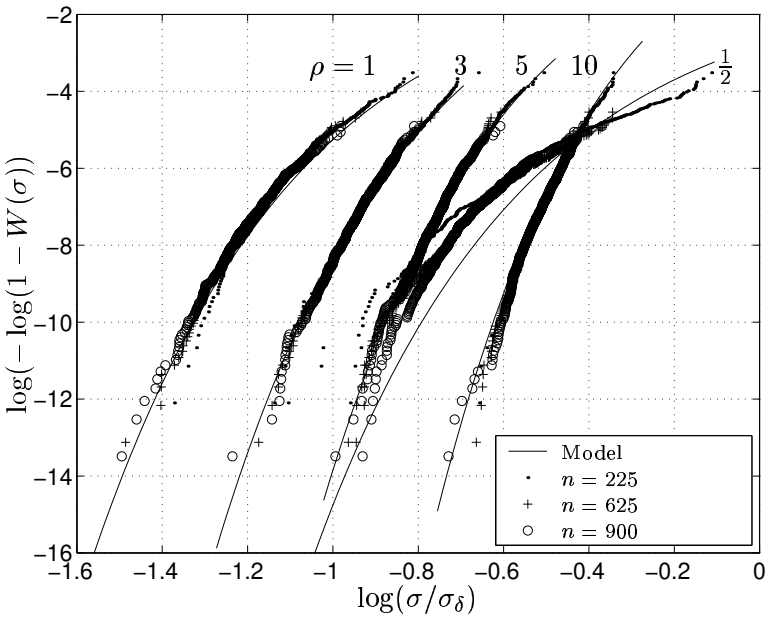

Figure 4. Weakest-link scaling phenomenon in 1D δ-bundles. The empirical weakest-link distributions, $\hat{W}_n(\sigma)$, for sizes $n = 225$, 625 and 900 collapse onto one master distribution, $\hat{W}(\sigma)$, for $\rho \geq 1$ but not for $\rho = 0.5$. Also shown is the characteristic distribution function, $W(\sigma)$, from the cluster growth model in Eq. (40).

and

$$\underline{F}(\sigma) = \begin{cases} 0 & \text{if } \sigma < 0, \\ 1 - 1/e & \text{if } 0 \leq \sigma < \sigma_\delta, \\ F(\sigma) & \text{if } \sigma_\delta \leq \sigma, \end{cases} \tag{21}$$

where $F(\sigma)$ is the original Weibull distribution, Eq. (1). The former reduces the strength of all fibers stronger than σ_δ to exactly σ_δ in the original Weibull distribution, and the latter weakens or pre-breaks to zero strength all fibers weaker than σ_δ. The simulation results in Figure 6 show that the δ-bundle strength distribution produced by $\overline{F}(\sigma)$ agrees nearly perfectly with that due to the original Weibull $F(\sigma)$ but the same is not true of $\underline{F}(\sigma)$ where a large strength reduction occurs.

3.2. Large variability in fiber strength (small ρ)

When ρ is small (large fiber variability), the cluster-driven breakdown mechanism is subdued by a dispersed failure mode in a δ-bundle. This is seen in snapshots of the fiber failure sequence in 1D HLLS and 2D HVLLS δ-bundles for $\rho = 1$, as shown in Figures 7 and 8, respectively.

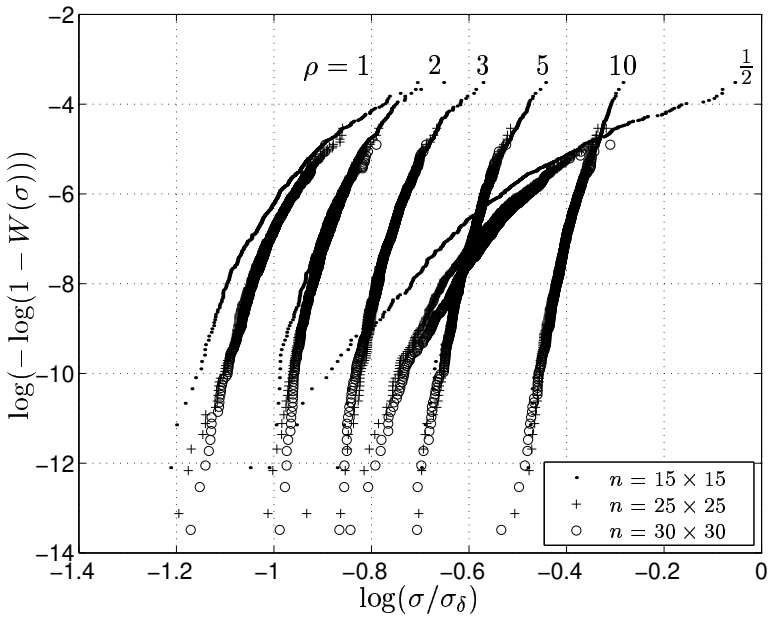

Figure 5. Weakest-link scaling phenomenon in 2D δ-bundles. The weakest-link distribution, $\hat{W}_n(\sigma)$, for composite sizes $n = 225$, 625 and 900 appears to converge onto one master distribution, $\hat{W}(\sigma)$, for $\rho > 1$.

A qualitative explanation for this is that the tendency to form and grow clusters is suppressed by the tendency to form breaks dispersedly, thereby undermining the ability of any one cluster to propagate. Instead, bundle failure results from the coalescence of small clusters and dispersed breaks. Thus, when the fiber strength variability is large, clusters of fiber breaks are less likely to propagate due to the presence of occasional strong fibers that impede growth. Also, many weak fibers fail under small applied loads causing the initial dispersed patterns.

Despite the dispersion of breaks in the failure mode of the 1D δ-bundles (Figure 7) with 30 fibers, there is convergence to a characteristic distribution $\hat{W}(\sigma)$ for sizes exceeding $n = 225$ (Figure 4). This suggests that fiber breakage, despite beginning dispersedly approaches clustered growth after a certain number of dispersed breaks have formed. This aspect will be revisited later.

To gain further insight into the behavior of the empirical distribution function for δ-bundle strength, $\hat{G}_n(\sigma)$, for small ρ, we have plotted $\hat{G}_n(\sigma)$ in Figure 9 under all three types of load-sharing: 1D HLLS, 2D HVLLS and ELS (equal load-sharing) as described in Section 1.2. The δ-bundles all have $n = 900$ fibers, and normal (Gaussian) coordinates have been used for plotting since the strength under ELS, a truly

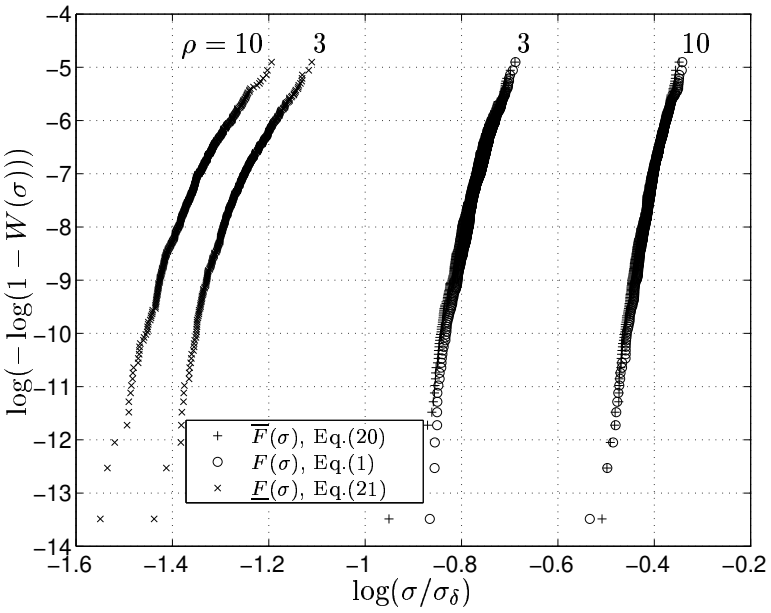

Figure 6. Dominance of the lower tail of the Weibull fiber strength distribution in determining δ-bundle strength for 2D HVLLS and larger ρ as seen from agreement between simulations for $\overline{F}(\sigma)$ and the original $F(\sigma)$ for $\rho = 3$ and 10.

dispersed failure mode, is very close to Gaussian (i.e., a straight line). As ρ decreases, the strength distributions for all three types of load-

Figure 7. Snapshots of the failure process in a median strength ($N = 500$) 2D HLLS δ-bundle with 30 Weibull fibers and $\rho = 1$ under periodic boundary conditions. ◯ intact fibers, ⊗ broken fibers, and ⊙ first fibers to fail after instability.

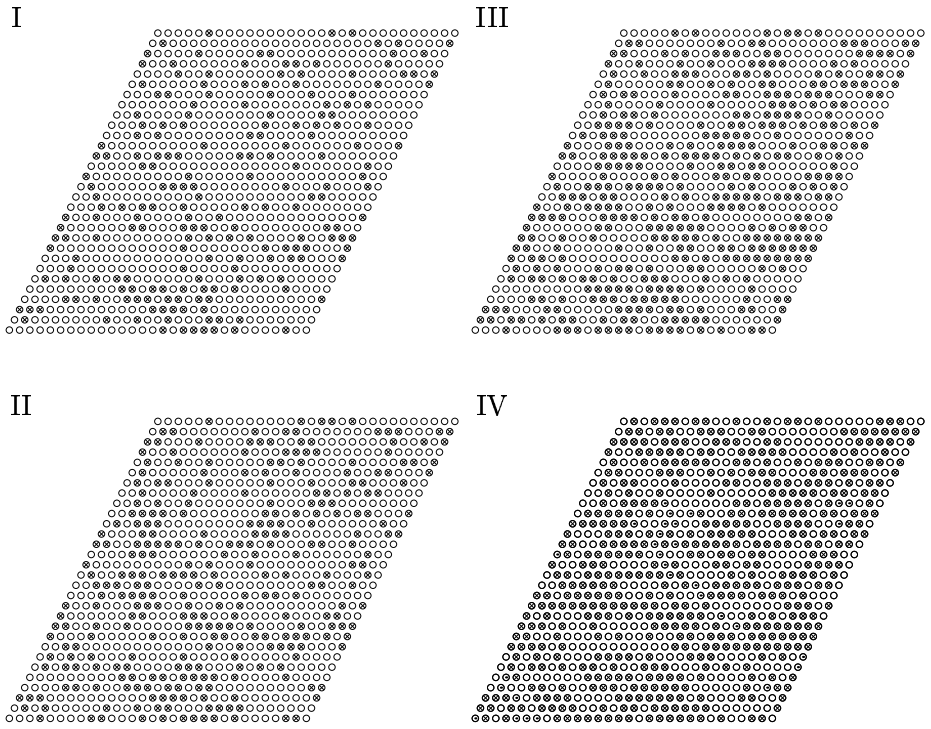

Figure 8. Snapshots of the failure process in a median strength ($N = 500$) 2D HVLLS δ-bundle with 900 Weibull fibers and $\rho = 1$ under periodic boundary conditions. ◯ intact fibers, ⊗ broken fibers, and ⊙ first fibers to fail after instability.

sharing converge. For 2D HVLLS the convergence is virtually complete for $\rho = 1$ and for 1D HLLS, the convergence improves dramatically between $\rho = 1$ and $\rho = 1/2$, though it is not quite complete even at $\rho = 1/2$. Remarkably, as ρ decreases, the details of the load sharing mechanism diminish in importance in determining the strength distribution. Also, the ELS strength distribution acts as a lower bound on the HVLLS distribution, becoming tight as ρ becomes small. It is an open question whether ELS bundles always have lower probability of failure than LLS bundles, as ρ decreases further.

Two cautionary points should be made. First, although the distributions for δ-bundle strength under HLLS and HVLLS approach those for ELS, the patterns of fiber breaks in terms of cluster sizes are not the same whereby ELS shows more dispersion. Second, if the bundle size n were increased by orders of magnitude, the reduction in variability for ELS is roughly $1/\sqrt{n}$, whereas for HVLLS and HLLS it may be milder. In fact, HVLLS and HLLS may ultimately produce slightly

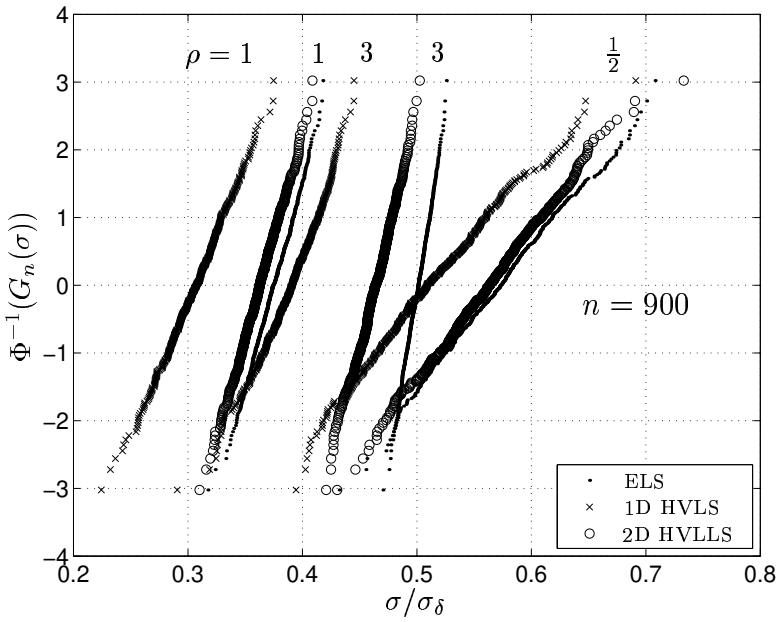

Figure 9. Comparison of empirical strength distributions, $\hat{G}_n(\sigma)$, for 900 fiber δ-bundles under ELS, 2D HVLLS and 1D HLLS on normal (Gaussian) probability coordinates.

weaker bundles than ELS since the scale of load-sharing over groups of fibers may be more limited than in ELS. Thus the large δ-bundle may act more like a chain of smaller δ-bundles, each roughly following ELS. We revisit this issue in Section 5.

For 2D HVLLS δ-bundles, when $0 < \rho \leq 1$, the strength distribution is dominated by the upper tail of the fiber strength distribution within the range of our simulations. In Figure 10, we compare the strength distributions produced by the upper and lower tail-modified Weibull distribution Eqs. (20) and (21) against those produced by the original Weibull distribution, Eq. (1). As ρ decreases, the upper tail dominance increases as the behavior becomes insensitive to the lower tail suggesting that cluster propagation is stalled by occasional strong fibers. This is the opposite to that seen in Figure 6 for larger ρ. Further investigation of this issue is considered in Section 5.

4. Analysis of Composite Strength Distribution for Large ρ

We now develop closed-form analytical approximations to the characteristic distribution function $W(\sigma)$ using a cluster growth approach as

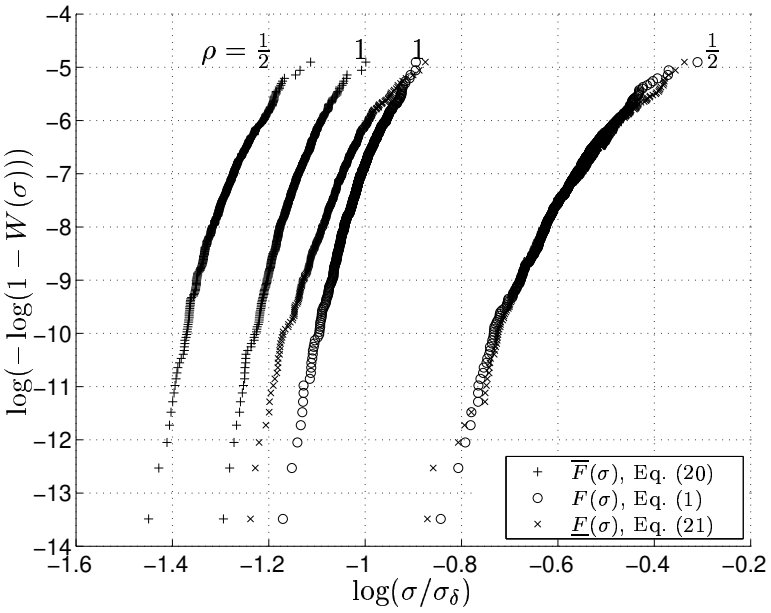

Figure 10. Dominance of the upper tail of the Weibull fiber strength distribution on the empirical characteristic distribution function, $\hat{W}(\sigma)$, for δ-bundles with 900 fibers and $\rho = 1$ and 1/2. Shown are the original Weibull $F(\sigma)$, $\overline{F}(\sigma)$ with strong fibers reduced in strength, and $\underline{F}(\sigma)$ with weaker fibers reduced to zero strength.

originally described in Smith (1980) and Phoenix and Smith (1983). The importance of this result is that the distribution function for the strength of a large composite with n fibers of length L becomes

$$\begin{aligned} H_{m,n}(\sigma) &\approx 1 - [1 - W(\sigma)]^{mn} \\ &\approx 1 - e^{-mnW(\sigma)}, \qquad \sigma \geq 0, \end{aligned} \tag{22}$$

where $m = L/\delta$ is the number of δ-bundles in the composite. Notably the resulting probability depends on the composite volume mn.

4.1. Characteristic distribution $W(\sigma)$ under 1D HLLS

To derive an approximation to $W(\sigma)$ in the case of 1D HLLS we model δ-bundle failure as a cascade of fiber failures. To begin, we approximate the probability such a cascade occurs, starting with the failure of a given fiber. The structure of such an event is that under stress σ, a given fiber fails, and its two immediate neighbors then suffer stress $K_1\sigma$, of which one fails. The pair of breaks formed causes one of the two adjacent overloaded neighbors to fail under stress $K_2\sigma$, the resulting triplet then fails one of its two overloaded neighbors under stress $K_3\sigma$, and so on

until all n fibers have failed. Thus, $W(\sigma)$ is approximately

$$\begin{aligned} W_n(\sigma) &\approx F(\sigma)\{1-[1-F(K_1\sigma)]^2\}\{1-[1-F(K_2\sigma)]^2\} \quad \cdots \\ &\qquad \{1-[1-F(K_{n-1}\sigma)]^2\} \\ &= \left\{1-\exp\left[-\left(\frac{\sigma}{\sigma_\delta}\right)^\rho\right]\right\} \prod_{r=1}^{n-1} \left\{1-\exp\left[-2\left(\frac{K_r\sigma}{\sigma_\delta}\right)^\rho\right]\right\}, \end{aligned} \tag{23}$$

where K_r is the stress concentration on the two fibers next to an r-cluster as approximated by Eq. (13), and $F(\sigma)$ is given by Eq. (1).

Simplifying assumptions are made in writing Eq. (23). First, only the failure of the fibers adjacent to an r-cluster are considered. Failure of fibers further away is ignored even though such fibers are overloaded. This is justified because, as r becomes large, the fibers neighboring the cluster carry twice as much load as the fibers sub-adjacent to it, according to Eq. (14). Thus for large ρ, the probability of failure of a sub-adjacent fiber without the failure of the adjacent fiber is negligible. Second, the formula assumes that fibers next to the cluster are virgin. In other words, in evaluating the probability of failure of an overloaded fiber at stress $K_r\sigma$, the event that it survived a lower stress $K_j\sigma$, $j < r$ is ignored. While the first assumption decreases the calculated probability of failure relative to the true one, the second assumption increases it. For large ρ, the errors thus committed are negligible.

While Eq. (23) can be used directly to estimate $W(\sigma)$ numerically for larger n, it is more illuminating to have a functional form for $W(\sigma)$ independent of n. We now derive such an approximation especially applicable in the lower tail (smaller σ/σ_δ). When $K_r\sigma \ll \sigma_\delta$ we have

$$1-\exp\left[-2\left(\frac{K_r\sigma}{\sigma_\delta}\right)^\rho\right] \approx 2\left(\frac{K_r\sigma}{\sigma_\delta}\right)^\rho \left[1-\left(\frac{K_r\sigma}{\sigma_\delta}\right)^\rho\right]. \tag{24}$$

This simplification is inaccurate when $K_r\sigma$ becomes comparable to σ_δ. In order to preserve accuracy in this range, we rewrite Eq. (23) as

$$\begin{aligned} W_\infty(\sigma) &\approx \left\{\left(\frac{\sigma}{\sigma_\delta}\right)^\rho \prod_{j=1}^{k(\sigma)-1}\left[2\left(\frac{K_j\sigma}{\sigma_\delta}\right)^\rho\right]\right\}\left\{\prod_{j=1}^{k(\sigma)-1}\left[1-\left(\frac{K_j\sigma}{\sigma_\delta}\right)^\rho\right]\right\} \\ &\qquad \times \left\{\prod_{j=k(\sigma)}^{\infty}\left[1-\exp\left(-2\left(\frac{K_j\sigma}{\sigma_\delta}\right)^\rho\right)\right]\right\} \\ &\equiv \left\{W_{k(\sigma)}(\sigma)\right\}\{\Psi_1(\sigma)\}\{\Psi_2(\sigma)\}, \end{aligned} \tag{25}$$

where $k(\sigma)$ is an appropriately chosen critical cluster size depending on σ, as we describe shortly. Also we have preserved the explicit

dependence on k of the first quantity, which can be written as

$$W_k(\sigma) = 2^{k-1}(K_1 K_2 \cdots K_{k-1})^{\rho} \left(\frac{\sigma}{\sigma_\delta}\right)^{k\rho}. \tag{26}$$

Note that the third product $\Psi_2(\sigma)$, in Eq. (25), is carried out to ∞ instead of n since the terms in the product converge very rapidly to unity and the product itself converges rapidly in n. Except for very small n this replacement has negligible effect and has the benefit of making $W(\sigma)$ explicitly independent of n.

One way to define $k(\sigma)$ might be to take it as the integer satisfying

$$F(K_{k-1}\sigma) < 1 - \frac{1}{e} \leq F(K_k\sigma). \tag{27}$$

This, however, leads to a discontinuous $W(\sigma)$ because the 2^{k-1} factor in Eq. (26) prevents $W(\sigma)$ from being continuous at exactly $\sigma/\sigma_\delta = 1/K_k$. Smooth transitions, however, do occur at certain values of σ where the right hand side of Eq. (26) has the same value for both k and $k+1$, i.e., for a transition σ such that

$$2^{k-1}(K_1 K_2 \cdots K_{k-1})^{\rho} \left(\frac{\sigma}{\sigma_\delta}\right)^{k\rho} = 2^{k}(K_1 K_2 \cdots K_{k})^{\rho} \left(\frac{\sigma}{\sigma_\delta}\right)^{(k+1)\rho}. \tag{28}$$

Taking the approximation Eq. (13) as the equality

$$K_r = \sqrt{\frac{b+r}{b}}, \tag{29}$$

we then have

$$\frac{\sigma}{\sigma_\delta} = \frac{2^{-1/\rho}}{K_k} = \frac{a}{\sqrt{k+b}}, \tag{30}$$

where

$$a = 2^{(\rho-1)/\rho}/\pi^{1/2} \quad \text{and} \quad b = 4/\pi. \tag{31}$$

When σ is decreased continuously the associated k cannot increase continuously since it takes on only integer values. If we relax this requirement and also permit k to vary continuously, we may replace σ/σ_δ in Eq. (26) in terms of k according to Eq. (30). In addition, substituting for K_r using Eq. (29) we have $W_k(\sigma)$ only as a function of k whereby

$$W_k = \frac{a^\rho}{(k+b)^{k\rho/2}} \prod_{r=1}^{k-1} (r+b)^{\rho/2}. \tag{32}$$

Evaluating the product in Eq. (32) yields

$$\begin{aligned}\prod_{r=1}^{k-1}(r+b)^{\rho/2} &= \exp\left\{\frac{\rho}{2}\sum_{r=1}^{k-1}\log(r+b)\right\} \\ &\approx \exp\left\{\frac{\rho}{2}\int_1^k \log(u+b)du - \frac{\rho}{4}\int_1^k \frac{1}{u+b}du\right\} \\ &= \left(\frac{(b+k)^{b+k-1/2}}{(b+1)^{b+1/2}}\right)^{\rho/2} \exp\left\{-\frac{\rho(k-1)}{2}\right\},\end{aligned} \tag{33}$$

so that

$$W_k = C(k+b)^{\phi}\exp\left\{-\beta(k+b)\right\}, \tag{34}$$

where

$$\begin{aligned}\beta &= \frac{\rho}{2}, \\ \phi &= \rho\left(\frac{b}{2}-\frac{1}{4}\right), \quad \text{and} \\ C &= a^{\rho}e^{\beta(b+1)}(1+b)^{-\beta(b+1/2)}.\end{aligned} \tag{35}$$

To get a relationship between W_k and σ, we use Eq. (30) relating k to σ, and upon simplification obtain

$$W_{k(\sigma)}(\sigma) = C\left(\frac{a\sigma_\delta}{\sigma}\right)^{2\phi}\exp\left\{-\beta\left(\frac{a\sigma_\delta}{\sigma}\right)^2\right\}. \tag{36}$$

Next we approximate $\Psi_1(\sigma)$ in Eq. (25). Using Eq. (30) we obtain

$$\begin{aligned}\Psi_1(\sigma) &= \prod_{j=1}^{k(\sigma)}\left[1-\left(\frac{K_j\sigma}{\sigma_\delta}\right)^{\rho}\right] \\ &\approx \exp\left\{-\sum_{j=1}^{k(\sigma)}\left(\frac{K_j\sigma}{\sigma_\delta}\right)^{\rho}\right\} \\ &\approx \exp\left\{-\frac{1}{2}\int_0^{k(\sigma)}(b+u)^{\rho/2}\left(\frac{\sigma}{a\sigma_\delta}\right)^{\rho}du\right\} \\ &\approx \exp\left\{-\left(\frac{a\sigma_\delta}{\sigma}\right)^2\frac{2}{2(\rho+2)}\left[1-b^{(\rho+2)/2}\left(\frac{\sigma}{a\sigma_\delta}\right)^{\rho+2}\right]\right\}.\end{aligned} \tag{37}$$

Finally we evaluate $\Psi_2(\sigma)$, the third product in Eq. (25), which is the probability of cluster stalling. Upon using Eq. (30) we obtain

$$\begin{aligned}\Psi_2(\sigma) &= \prod_{j=k(\sigma)}^{\infty}\left[1-\exp\left\{-2\left(\frac{K_j\sigma}{\sigma_\delta}\right)^\rho\right\}\right] \\ &\approx \exp\left\{-\sum_{j=k(\sigma)}^{\infty}\exp\left\{-2\left(\frac{K_j\sigma}{\sigma_\delta}\right)^\rho\right\}\right\} \\ &\approx \exp\left\{-\int_{k(\sigma)}^{\infty}\exp\left\{-(b+u)^{\rho/2}\left(\frac{\sigma}{a\sigma_\delta}\right)^\rho\right\}du\right\} \\ &= \exp\left\{-\frac{2}{\rho}\Gamma(2/\rho,1)\left(\frac{a\sigma_\delta}{\sigma}\right)^2\right\},\end{aligned} \tag{38}$$

where

$$\Gamma(p,1) = \int_1^\infty e^{-u}u^{p-1}du \tag{39}$$

is the incomplete gamma function. Substituting Eqs. (36), (37) and (38) into Eq. (25), i.e., $W_\infty(\sigma) \approx W_k(\sigma)\Psi_1(\sigma)\Psi_2(\sigma)$, keeping only the dominant term in Eq. (37) and dropping the subscript '∞', we obtain

$$W(\sigma) \approx C\left(\frac{a\sigma_\delta}{\sigma}\right)^{2\phi}\exp\left\{-B\beta\left(\frac{a\sigma_\delta}{\sigma}\right)^2\right\}, \tag{40}$$

where

$$B = 1+\left(\frac{2}{\rho}\right)^2\left[\frac{\rho}{2(\rho+2)}+\Gamma(2/\rho,1)\right], \tag{41}$$

and all other constants are as defined in Eq. (31) and Eq. (35). Note the emergence of the quantity $\rho/2$ as an important parameter in B. As ρ decreases below 2, B begins to grow rapidly, which lowers $W(\sigma)$.

Since there are n fibers in a δ-bundle, a cascade can originate from any one of them, and these events are taken as being statistically independent. This results in the approximation Eq. (18), and through Eq. (3), to $H_{m,n}(\sigma)$ for the full composite as given by Eq. (22).

To investigate the success of this result we compare $W(\sigma)$ to $\hat{W}(\sigma)$, which results from the convergence of the simulated $\hat{W}_n(\sigma)$ of Eq. (19) with increasing n. Figure 4 shows $W(\sigma)$ from Eq. (40) together with $\hat{W}(\sigma)$ from the Monte Carlo simulations. No adjustable parameters are involved. For $\rho = 1, 3, 5$, and 10, the calculated and simulated distributions are in remarkable agreement. For $\rho = 0.5$ the agreement suddenly weakens where no n-independent $\hat{W}(\sigma)$ appears. This lack of

agreement is consistent with our earlier observations in Figure 9 where the distribution $\hat{G}_n(\sigma)$ for δ-bundle strength was close to that for ELS, which has a dispersed fiber failure mode. The value $\rho = 2$ does not emerge as having a dominating effect. Surprisingly the model seems to apply well for $\rho = 1$, and Figure 4 does not rule out its application for $\rho = 1/2$. This issue is revisited in Section 5.

4.2. Size effects for critical cluster and composite strength under HLLS

We next examine the size effect for the characteristic composite strength. That is, for fixed probability of failure p, we ask how the composite strength for the pth quantile scales in terms of number of fibers n and length $L = m\delta$ where m is the number of δ-bundles in the composite. We take $p = 1 - 1/e = 0.632$, which would correspond to the Weibull scale parameter for composite strength in a Weibull approximation to $H_{m,n}(\sigma)$. We examine the dependence of the critical cluster size on n at failure probability level p, and want to know the size of the critical cluster at the point where it becomes unstable. Extending these results to the full composite is simply a matter of replacing n by mn.

We know that

$$G_n(\sigma) \approx 1 - [1 - W(\sigma)]^n \approx 1 - e^{-nW(\sigma)}. \tag{42}$$

Equating this further to $1-e^{-1}$, we find that the characteristic δ-bundle strength, denoted σ_c^*, is the stress σ solving $W(\sigma) = 1/n$ where $W(\sigma)$ is given by Eq. (40). While this equation can be inverted asymptotically to get σ_c^*, it turns out to be useful to think also in terms of a critical cluster size k^* associated with failure probability p. This is obtained by setting $W_k = 1/n$ in Eq. (34), that is, k^* must solve

$$(k^* + b)^{-\phi} e^{\beta(k^*+b)} = nC, \tag{43}$$

which is an implicit relation between k^* and n.

To obtain an explicit relation between k^* and n, we observe that

$$-\phi \log(k^* + b) + \beta(k^* + b) = \log(nC). \tag{44}$$

Substituting $k^* + b = (1 + \epsilon)\log(nC)/\beta$ and using $\log(1 + \epsilon) \approx \epsilon$ gives the critical cluster size k^* for a δ-bundle approximately as

$$k^* + b = (1 + \epsilon)\frac{\log(nC)}{\beta}, \tag{45}$$

where

$$\epsilon \approx \frac{\phi\,\{\log[\log(nC)] - \log(\beta)\}}{\log(nC) - \phi}, \tag{46}$$

and log is the Napierian logarithm. To obtain an integer valued k^*, one must round up the k^* from Eq. (45) to the next largest integer. To obtain k^* for the full composite simply replace n by mn in Eq. (45).

To obtain the characteristic strength σ_c^* of a δ-bundle we first use Eq. (30) to recast Eq. (45) in terms of σ, yielding the critical stress

$$\sigma^* = a\sigma_\delta \sqrt{\frac{\beta}{\log(nC)(1+\epsilon)}}. \tag{47}$$

This expression, however, does not account for the crack stalling probability $\Psi_2(\sigma)$. It can be interpreted as the stress associated with *formation* of a cluster of critical size k^* where the probability of further propagation becomes likely but not guaranteed to be catastrophic. Including $\Psi_2(\sigma)$ as well yields the characteristic δ-bundle strength

$$\sigma_c^* = a\sigma_\delta \sqrt{\frac{B\beta}{\log(nC)(1+\epsilon(B\beta))}}, \tag{48}$$

where $\epsilon(B\beta)$ is given by Eq. (46) with β replaced by $B\beta$. Again, to obtain the characteristic composite strength, replace n by mn in Eq. (48).

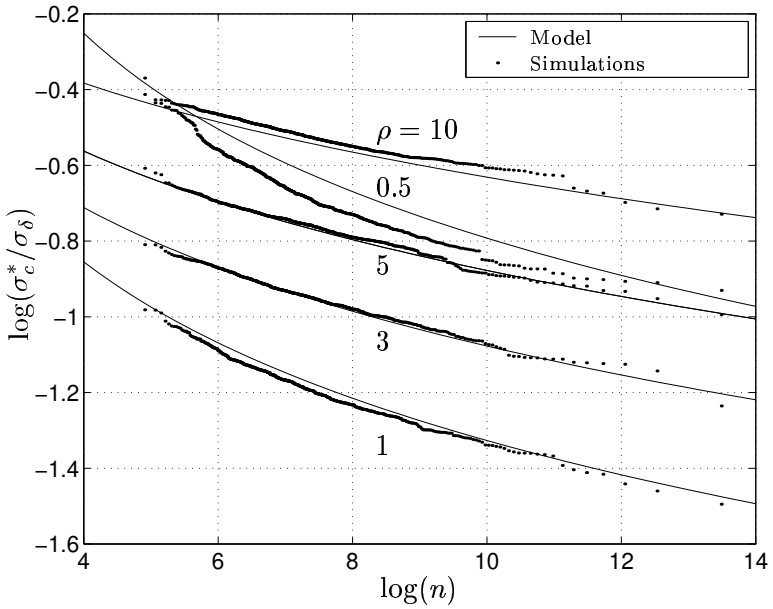

Figure 11. Comparison of Eq. (47) with size effect predicted from the simulated empirical strength distributions of a 900-fiber δ-bundle under 1D HLLS.

Figure 11 shows plots of the characteristic strength σ_c^* versus δ-bundle size n based on Eq. (48). The agreement is good even for $\rho = 1/2$, which did not show failure by cluster growth over this range of n.

4.3. Characteristic distribution $W(\sigma)$ under 2D HVLLS

The approach taken to approximate $W(\sigma)$ for 2D HVLLS is identical to that used in 1D HLLS except that the possible geometries of break clusters introduce additional complexities. We model the cascade event defining $W(\sigma)$ as the formation of a break cluster at stress σ that goes unstable. The diameter D of a tight circular cluster of r breaks was defined earlier as $\pi D^2/4 = r$. The circumference of the circle, $\pi D = \sqrt{4\pi r}$ is approximately the number of intact fibers surrounding this r-cluster. Let N_r be the number of these neighbors that are severely overloaded. The first step is the failure of a given fiber in the δ-bundle under σ, followed by the failure of one of its $N_1 = 6$ equally overloaded neighbors under stress $K_1\sigma$. The resulting pair of fiber breaks has eight intact neighbors of which only $N_2 = 2$ are severely overloaded under stress $K_2\sigma$. The next likely event is the failure of one of these, to form a break triplet with $N_3 = 3$ severely overloaded neighbors, of which one fails, and so on. The critical event is thus the evolution of a growing "tight" r-cluster (Figure 12), with each added break being the failure of one of the N_r severely overloaded fibers surrounding it.

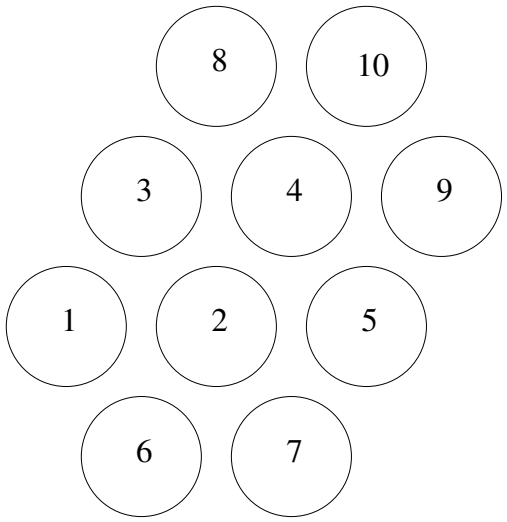

i	K_i
1	1.0000
2	1.1046
3	1.2337
4	1.2828
5	1.3205
6	1.3644
7	1.5889
8	1.4107
9	1.4596
10	1.6163

Figure 12. One possible sequence of tight cluster growth to 10 fiber breaks in a hexagonal fiber array. The numbers $(1, 2, \ldots, 10)$ indicate break sequence. Also included are the associated stress concentrations computed under HVLLS.

As in the 1D case, we write this as

$$W_n(\sigma) \approx F(\sigma)\{1-[1-F(K_1\sigma)]^{N_1}\} \times \{1-[1-F(K_2\sigma)]^{N_2}\} \cdots \{1-[1-F(K_{n-1}\sigma)]^{N_{n-1}}\}, \tag{49}$$

where K_r is the stress concentration on the N_r most severely overloaded neighbors of a tight r-cluster. We introduce a two-parameter, power law to account for the actual number of neighbors at high risk,

$$N_r = \eta r^{\gamma}, \tag{50}$$

with parameters η and γ satisfying $\eta > 0$ and $0 < \gamma \leq 1/2$. This power form for N_r is essential for $W_n(\sigma)$ in Eq. (49) to agree with the simulated $\hat{W}(\sigma)$ distribution as ρ becomes small. Observe that if $\eta = \sqrt{4\pi} \approx 3.55$ and $\gamma = 1/2$, then N_r is simply the total number of intact fibers surrounding a circular r-cluster.

Applying approximations as in Section 4.1 we rewrite Eq. (49) as

$$\begin{aligned} W_\infty(\sigma) &\approx \left\{\left(\frac{\sigma}{\sigma_\delta}\right)^{\rho} \prod_{j=1}^{k(\sigma)-1}\left[N_j\left(\frac{K_j\sigma}{\sigma_\delta}\right)^{\rho}\right]\right\}\left\{\prod_{j=1}^{k(\sigma)-1}\left[1-\frac{N_j}{2}\left(\frac{K_j\sigma}{\sigma_\delta}\right)^{\rho}\right]\right\} \\ &\quad \times \left\{\prod_{j=k(\sigma)}^{\infty}\left[1-\exp\left(-N_j\left(\frac{K_j\sigma}{\sigma_\delta}\right)^{\rho}\right)\right]\right\} \\ &\equiv \left\{W_{k(\sigma)}(\sigma)\right\}\{\Psi_1(\sigma)\}\{\Psi_2(\sigma)\}. \end{aligned} \tag{51}$$

Again the explicit dependence on k in the first product $W_{k(\sigma)}(\sigma)$ is retained, and it may be written as

$$W_k(\sigma) = N_1 N_2 \cdots N_{k-1}(K_1 K_2 \cdots K_{k-1})^{\rho}\left(\frac{\sigma}{\sigma_\delta}\right)^{k\rho}. \tag{52}$$

As in the case of 1D, we relate σ to k by setting $W_k(\sigma) = W_{k+1}(\sigma)$. Doing so and recalling Eq. (16) for K_r, which we rewrite as

$$K_r = \sqrt{\frac{\sqrt{r}+b}{b}}, \tag{53}$$

we obtain

$$\frac{\sigma}{\sigma_\delta} = a k^{-\gamma/\rho}(\sqrt{k}+b)^{-1/2}, \tag{54}$$

where

$$a = \sqrt{b}/\eta^{1/\rho} \quad \text{and} \quad b = \pi^{3/2}/2. \tag{55}$$

Using Eqs. (50), (53) and (54) in Eq. (52) and simplifying we obtain

$$W_k = \frac{[(k-1)!]^\gamma \prod_{j=0}^{k-1}(\sqrt{j}+b)^{\rho/2}}{\eta k^{k\gamma}(\sqrt{k}+b)^{k\rho/2}}. \tag{56}$$

We can evaluate Eq. (56) as follows: By Stirling's formula,

$$(k-1)! \approx \sqrt{2\pi}k^{k-1/2}e^{-k}. \tag{57}$$

Also,

$$\begin{aligned}
\prod_{j=0}^{k-1}(\sqrt{j}+b) &= \exp\left\{\sum_{j=0}^{k-1}\log(\sqrt{j}+b)\right\} \\
&\approx \exp\left\{\int_{u=0}^{k}\log(\sqrt{u}+b)du - \int_{u=0}^{k}\frac{1}{2}\frac{d\log(\sqrt{x}+b)}{dx}dx\right\} \\
&= (\sqrt{k}+b)^{k-b^2-1/2}b^{(b^2+1/2)} \\
&\quad \times \exp\left\{-\frac{1}{2}(\sqrt{k}+b)^2 + 2b(\sqrt{k}+b) - \frac{3b^2}{2}\right\}.
\end{aligned} \tag{58}$$

Using these two approximations in Eq. (56) and noting that

$$k^{-\gamma/2} = (\sqrt{k}+b)^{-\gamma}\left[1 - \frac{b}{\sqrt{k}+b}\right]^{-\gamma} \approx (\sqrt{k}+b)^{-\gamma}, \tag{59}$$

while

$$\exp\{\gamma k\} = \exp\{\gamma[(\sqrt{k}+b)^2 - 2b(\sqrt{k}+b) + b^2]\}, \tag{60}$$

we may reduce Eq. (56) to

$$W_k = C(\sqrt{k}+b)^{-\varphi}\exp\left\{-\beta_1\left(\sqrt{k}+b-\frac{\beta_2}{2\beta_1}\right)^2\right\}, \tag{61}$$

where

$$\begin{aligned}
C &= \frac{(2\pi)^{\frac{\gamma}{2}}}{\eta}b^{(\rho/2)(b^2+1/2)}\exp\left\{-b^2\left(\frac{3\rho}{4}+\gamma\right)+\frac{\beta_2^2}{4\beta_1}\right\}, \\
\varphi &= \gamma + (\rho/2)(b^2+\frac{1}{2}), \\
\beta_1 &= \frac{\rho+4\gamma}{4}, \quad \text{and} \\
\beta_2 &= b(\rho+2\gamma).
\end{aligned} \tag{62}$$

To get an expression in terms of σ, we first write Eq. (54) as

$$\frac{\sigma}{a\sigma_\delta} = (\sqrt{k}+b)^{-2\beta_1/\rho} \quad \left[1 - \frac{b}{\sqrt{k}+b}\right]^{-2\gamma/\rho}, \tag{63}$$

which can approximately be inverted to give

$$\sqrt{k}+b \approx \left(\frac{\sigma}{a\sigma_\delta}\right)^{-\rho/(2\beta_1)} + \frac{b\gamma}{\beta_1} + \frac{b^2\gamma}{2\beta_1^2}\left(\beta_1-\gamma\right)\left(\frac{\sigma}{a\sigma_\delta}\right)^{\rho/(2\beta_1)}. \tag{64}$$

Dropping the last term leads to

$$\frac{\sigma}{a\sigma_\delta} = \left(\sqrt{k}+b-\frac{b\gamma}{\beta_1}\right)^{-2\beta_1/\rho}, \tag{65}$$

which for given σ results in a slightly lower value of k as compared to Eq. (64). Substituting Eq. (64) into Eq. (61) for W_k gives

$$W_{k(\sigma)}(\sigma) = C\Omega_1(\sigma)\left(\frac{\sigma}{a\sigma_\delta}\right)^{\varphi\rho/(2\beta_1)} \exp\left\{-\beta_1\Theta_1(\sigma)\left(\frac{a\sigma_\delta}{\sigma}\right)^{\rho/\beta_1}\right\}, \tag{66}$$

where

$$\Omega_1(\sigma) = \left[1 + \frac{b\gamma}{\beta_1}\left(\frac{\sigma}{a\sigma_\delta}\right)^{\rho/(2\beta_1)} + \frac{b^2\gamma}{2\beta_1^2}\left(\beta_1-\gamma\right)\left(\frac{\sigma}{a\sigma_\delta}\right)^{\rho/\beta_1}\right]^{-\varphi}, \tag{67}$$

and

$$\Theta_1(\sigma) = \left[1 - \frac{b\rho}{2\beta_1}\left(\frac{\sigma}{a\sigma_\delta}\right)^{\rho/(2\beta_1)} + \frac{b^2\gamma}{2\beta_1^2}\left(\beta_1-\gamma\right)\left(\frac{\sigma}{a\sigma_\delta}\right)^{\rho/\beta_1}\right]^2. \tag{68}$$

Next we approximate the second product $\Psi_1(\sigma)$ in Eq. (51) as

$$\begin{aligned}
\Psi_1(\sigma) &= \prod_{j=0}^{k(\sigma)-1}\left[1 - \frac{N_j}{2}\left(\frac{K_j\sigma}{\sigma_\delta}\right)^\rho\right] \\
&\approx \exp\left\{-\sum_{j=0}^{k(\sigma)-1}\frac{N_j}{2}\left(\frac{K_j\sigma}{\sigma_\delta}\right)^\rho\right\} \\
&\approx \exp\left\{-\frac{1}{2}\left(\frac{\sigma}{a\sigma_\delta}\right)^\rho \int_0^{k(\sigma)} u^\gamma(\sqrt{u}+b)^{\rho/2}du\right\} \\
&\approx \exp\left\{-\frac{1}{2(\beta_1+1)}\Theta_2(\sigma)\left(\frac{a\sigma_\delta}{\sigma}\right)^{\frac{\rho}{\beta_1}}\right\},
\end{aligned} \tag{69}$$

where the last step involves applying Eq. (64) and keeping only the dominant terms, and where

$$\Theta_2(\sigma) = 1 - \frac{b\rho(\beta_1+1)}{2\beta_1(2\beta_1+1)}\left(\frac{\sigma}{a\sigma_\delta}\right)^{\frac{\rho}{2\beta_1}}. \tag{70}$$

Finally we evaluate the third product $\Psi_2(\sigma)$ in Eq. (51) as

$$\begin{aligned}\Psi_2(\sigma) &= \prod_{j=k(\sigma)}^{\infty} 1 - \exp\left(-N_j\left(\frac{K_j\sigma}{\sigma_\delta}\right)^{\rho}\right) \\ &\approx \exp\left\{-\sum_{j=k(\sigma)}^{\infty}\exp\left\{N_j\left(\frac{K_j\sigma}{\sigma_\delta}\right)^{\rho}\right\}\right\} \\ &\approx \exp\left\{-\int_{k(\sigma)}^{\infty}\exp\left\{-u^{\gamma}(\sqrt{u}+b)^{\rho/2}\left(\frac{\sigma}{a\sigma_\delta}\right)^{\rho}\right\}du\right\} \\ &\approx \exp\left\{-\frac{1}{\beta_1}\Gamma\left(\frac{1}{\beta_1},1\right)\Theta_3(\sigma)\left(\frac{a\sigma_\delta}{\sigma}\right)^{\rho/\beta_1}\right\},\end{aligned} \tag{71}$$

where

$$\Theta_3(\sigma) = 1 - \frac{b\rho}{4\beta_1}\frac{\Gamma\left(\frac{1}{2\beta_1},1\right)}{\Gamma\left(\frac{1}{\beta_1},1\right)}\left(\frac{\sigma}{a\sigma_\delta}\right)^{\rho/(2\beta_1)}. \tag{72}$$

Multiplying $W_k(\sigma)$, $\Psi_1(\sigma)$, and $\Psi_2(\sigma)$ in Eq. (51) and dropping the subscript '∞' finally gives our main result

$$W(\sigma) = C\Omega_1(\sigma)\left(\frac{\sigma}{a\sigma_\delta}\right)^{\varphi\rho/(2\beta_1)}\exp\left\{-\Omega_2(\sigma)\left(\frac{a\sigma_\delta}{\sigma}\right)^{\rho/\beta_1}\right\}, \tag{73}$$

where

$$\Omega_2(\sigma) = \beta_1\Theta_1(\sigma) + \frac{\Omega_1^{-\frac{1}{\varphi}}}{2}\Theta_2(\sigma) + \Gamma\left(\frac{1}{\beta_1},1\right)\frac{\Theta_3(\sigma)}{\beta_1}. \tag{74}$$

Figure 13 compares two versions of $W(\sigma)$ in Eq. (73) against $\hat{W}(\sigma)$ from the Monte Carlo simulations, for $\rho = 1, 2, 3, 5$, and 10. The dashed lines (Model 1) assume $\gamma = 1/2$ and $\eta = \sqrt{4\pi} = 3.55$ as is the case in Eq. (50) if we assume all fibers in the first ring around the cluster are equally at risk of failure. The solid lines (Model 2) assume γ and η values corresponding to the respective ρ values as shown in the table within the figure. The fit in the dashed line case, which is excellent for $\rho = 20$ (not shown) and quite good for $\rho = 10$, rapidly deteriorates for

$\rho \leq 5$. However, except for $\rho = 1$ the agreement is excellent when γ and η are adjusted as shown in the table. This suggests that the growth in the number of neighbors to the cluster at high risk of failure must be retarded after the first three or four breaks. For $\rho \leq 3$ it was retarded completely by setting $\gamma = 0$ and $\eta = 6$ so that the number of neighbors remained fixed at 6 regardless of the cluster size.

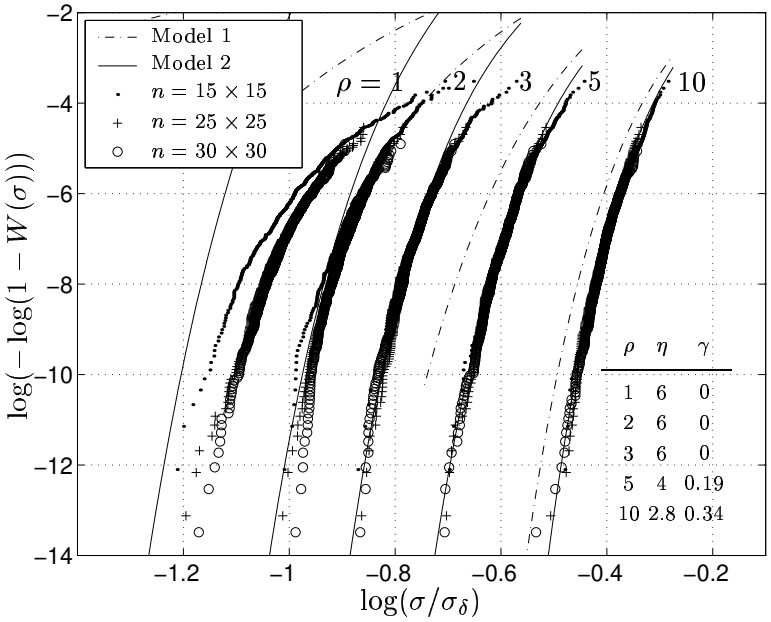

Figure 13. Comparison of the theoretical $W(\sigma)$ from the cluster growth model under 2D HVLLS and Weibull fibers with the empirical version $\hat{W}(\sigma)$ obtained from simulations. Model 1 assumes $\eta = \sqrt{4\pi}$ and $\gamma = 0.5$ for all ρ. In Model 2, the parameters η and γ are adjusted for each ρ to provide the best fit as shown in the table. Results corresponding to $\rho = 0.5$ are not shown because the plots of $W(\sigma)$ for both models lie off scale.

Many approximations were made in deriving $W(\sigma)$ in Eq. (73), but using the root equation, Eq. (49), does not improve the agreement with the simulations. Furthermore we have assumed the clusters are round, when in reality they will become increasingly irregular as ρ is decreased. Thus for moderate ρ, i.e., $2 < \rho < 10$, this irregularity may mean that relatively fewer of the neighbors should be viewed as highly stressed, perhaps only those that protrude the most into the cluster. The emergence of powers of γ less than $1/2$ for smaller ρ may also mean that the cluster roughness around the perimeter has fractal character as it grows and this somehow determines the effective number of neighbors at risk. In Section 6 we will suggest another possible explanation for

the adjustment involving decreasing the value of γ in Eq. (50) for N_r. Note also that the parameter $\beta_1 = (\rho + 4\gamma)/4$ plays a role in the behavior of $W(\sigma)$ through $\Omega_2(\sigma)$, Eq. (74), as ρ and γ diminish. Curiously, when $\gamma = 0$ we have $\beta_1 = \rho/4$ suggesting that the value $\rho = 4$ has special significance, as is also pursued further in Section 6. We find that $\Omega_2(\sigma)$ starts to increase rapidly when ρ diminishes below 4 reflecting an increased cluster stalling probability. This has the effect of decreasing $W(\sigma)$, and thus, the probability of failure, though the effect is not strong enough to explain the behavior of the simulations for small ρ in Figure 13.

The weakness of the fit for $\rho = 1$ is consistent with the earlier observation in Figure 9 that once ρ decreases below about 2, the δ-bundle failure distribution develops strong Gaussian character as seen under ELS, which is truly a dispersed failure mode.

4.4. Size effect for critical cluster and composite strength under HVLLS

We now derive formulas for the variation of the critical cluster size k^* with the size n of δ-bundles under 2D HVLLS and at failure probability level $p = 1 - 1/e$. We then derive the dependence of the characteristic δ-bundle strength σ_c^* on n. Converting this result to apply to the full composite only requires replacing n by mn.

The first step is to set $W_k = 1/n$ or, using Eq. (61), we have

$$C\left(\sqrt{k}+b\right)^{\varphi}\exp\left\{\beta_1\left(\sqrt{k}+b-\frac{\beta_2}{2\beta_1}\right)^2\right\} = nC. \tag{75}$$

For moderate k^*, we note that $\sqrt{k^*} + b$ is close to $\beta_2/2\beta_1$, which makes the exponential function in Eq. (75) amenable to a power series expansion. Asymptotic inversion leads to

$$\log\left(\sqrt{k^*}+b\right) = \frac{\log(nC) + log(\omega_1)}{\varphi}, \tag{76}$$

where the correction term $\log(\omega_1)$ grows slowly with $\log(nC)$ following

$$\log(\omega_1) = \frac{-\frac{\beta_2^2}{4\beta_1}\left[\frac{\log(nC)}{\varphi} - \log\left(\frac{\beta_2}{2\beta_1}\right)\right]^2}{1 + \frac{\beta_2^2}{4\beta_1\varphi}\left[\frac{\log(nC)}{\varphi} - \log\left(\frac{\beta_2}{2\beta_1}\right)\right]}. \tag{77}$$

The correction term ω_1, while small, can have a major effect on the resulting k^*. The above formula for k^* works for a wide range of n (e.g.

$n < 10^9$). However, for larger n, an expansion arises of the form

$$\sqrt{k^*} + b = \left(\sqrt{\frac{\log(nC)}{\beta_1}} + \frac{\beta_2}{2\beta_1} \right) (1 - \omega_2), \tag{78}$$

where the correction term ω_2 is

$$\omega_2 = \frac{\varphi \log \left(\sqrt{\frac{\log(nC)}{\beta_1}} + \frac{\beta_2}{2\beta_1} \right)}{\varphi + 2\log(nC) + \frac{\beta_2}{\beta_1} \sqrt{\frac{\log(nC)}{\beta_1}}}. \tag{79}$$

For astronomical n such as $n > 10^{25}$ we have

$$\sqrt{k^*} + b = \sqrt{\frac{\log(nC)}{\beta_1}}. \tag{80}$$

Substituting for k^* in terms of σ^* we estimate the size effect for the stress when the critical cluster forms. From Eqs. (65) and (76) we get

$$\sigma^* \approx a\sigma_\delta \left((nC\omega_1)^{1/\varphi} - \frac{b\gamma}{\beta_1} \right)^{-2\beta_1/\rho}. \tag{81}$$

For extremely large n, Eqs. (65) and (78) lead to

$$\sigma^* \approx a\sigma_\delta \left(\left(\sqrt{\frac{\log(nC)}{\beta_1}} + \frac{\beta_2}{2\beta_1} \right) (1 - \omega_2) - \frac{b\gamma}{\beta_1} \right)^{-2\beta_1/\rho}. \tag{82}$$

Finally, as $n \to \infty$, this behaves as

$$\sigma^* = a\sigma_\delta \left(\frac{\beta_1}{\log(nC)} \right)^{\beta_1/\rho}. \tag{83}$$

To obtain the characteristic stress for composite failure, σ_c^*, we must account for $\Psi_1(\sigma)$ and $\Psi_2(\sigma)$ leading to complex expressions. We estimate the main effect by noting that $\Omega_2(\sigma) \to B$ as $\sigma \to 0$ where

$$B = 1 + \frac{1}{2\beta_1(\beta_1 + 1)} + \frac{1}{\beta_1^2} \Gamma \left(\frac{1}{\beta_1}, 1 \right). \tag{84}$$

Thus for large n we may obtain σ_c^* from σ^* upon replacing $\log(nC)/\beta_1$ by $\log(nC)/(B\beta_1)$ in Eqs. (82) and (83). For smaller n, of the order used in our simulations, and larger values of ρ we can still use Eq. (81) for σ_c^*. For smaller ρ, say $\rho \leq 5$ where B differs appreciably from one, Eqs. (82) and (83) may be applied but are likely to be very conservative as $B\beta_1$ is a poor reflection of the full effect of $\Omega_2(\sigma)$ in Eq. (73).

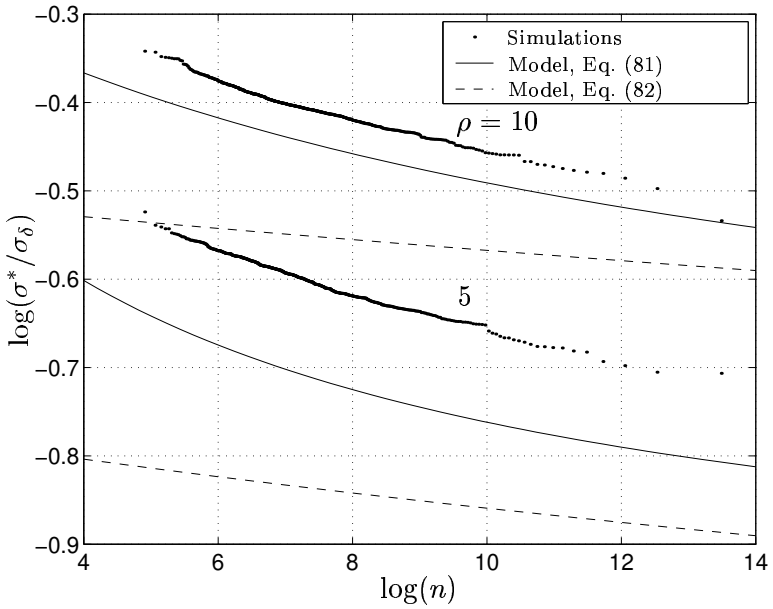

Figure 14. Comparison of the size effect predicted by the cluster growth model, Eqs. (81) and (82), with that derived from a $\hat{W}(\sigma)$ interpretation of the empirical strength distributions of a 900 fiber δ-bundle under 2D HVLLS.

Figure 14 shows a plot of σ_c^* given by Eq. (81) against the size effect predicted using simulations from the δ-bundles of size $n = 900$ as though they posses weakest link character in terms of $\hat{W}(\sigma)$, as is supported by Figure 13. The size range covered is $100 < n < 1,000,000$, which is the relevant range for Eq. (81). Clearly the formula works well for $\rho = 10$ and reasonably well for $\rho = 5$, but breaks down for smaller ρ, because of the above mentioned lack of treatment of the cluster stalling probability in the derivation. For extremely large n, Eq. (82) with the $B\beta_1$ modification shows the anticipated poorer performance. One one hand, discrepancies in Figure 14 may be due approximation errors, but on the other hand this could also serves to point out that composites of the size that can presently be treated by Monte Carlo simulation may not reveal the true size effect as might be relevant in applications.

4.5. Power-law fiber strength and δ-bundle behavior

In Section 4.1, we observed for 1D HLLS that the tight cluster growth model accurately predicts the empirical strength distribution for $\rho \geq 1$, but not for $\rho < 1$. In 2D HVLLS, when the fiber strength is Weibull, Eq. (1), the tight cluster growth mode does not seem to apply to $\rho < 2$

as seen in Figure 13. These departures may be due to non-tightness of cluster growth, or to the presence of occasional strong fibers, or both.

To resolve this we consider a cluster growth failure model for a δ-bundle with fiber strength that follows a power-law distribution, $F_p(\sigma)$, given by Eq. (2). Using $F_p(\sigma)$ in the arguments to develop Eq. (51), we have

$$\begin{aligned} W_\infty(\sigma) &\approx \left\{ \left(\frac{\sigma}{\sigma_\delta}\right)^\rho \prod_{j=1}^{k(\sigma)-1} \left[N_j \left(\frac{K_j \sigma}{\sigma_\delta}\right)^\rho \right] \right\} \\ &\quad \times \left\{ \prod_{j=k(\sigma)}^{k_m(\sigma)} \left[1 - \left(1 - \left(\frac{K_j \sigma}{\sigma_\delta}\right)^\rho \right)^{N_j} \right] \right\} \\ &\equiv \left\{ W_{k(\sigma)}(\sigma) \right\} \left\{ \Psi_2(\sigma) \right\}, \end{aligned} \tag{85}$$

where $k_m(\sigma)$ is such that $K_{k_m(\sigma)}\sigma/\sigma_\delta = 1$. Here $W_{k(\sigma)}(\sigma)$ is still given by Eq. (66), but the factor $\Psi_2(\sigma)$ is different and is approximated as

$$\Psi_2(\sigma) = \exp\left\{ -\frac{4b^2}{\rho} \Theta_2(\sigma) \left(\frac{\sigma_\delta}{\sigma}\right)^\rho \right\} \tag{86}$$

where

$$\begin{aligned} \Theta_2(\sigma) &= B\left(\eta k^\gamma(\sigma)+1, \frac{4}{\rho}\right) \left\{ 1 - I_{\left(\sqrt{\frac{k(\sigma)+1}{b}}\sigma\right)^\rho} \left(\eta k^\gamma(\sigma)+1, \frac{4}{\rho}\right) \right\} \\ &\quad - \left(\frac{\sigma}{\sigma_\delta}\right)^2 B\left(\eta k^\gamma(\sigma)+1, \frac{2}{\rho}\right) \left\{ 1 - I_{\left(\sqrt{\frac{k(\sigma)+1}{b}}\sigma\right)^\rho} \left(\eta k^\gamma(\sigma)+1, \frac{2}{\rho}\right) \right\} \end{aligned} \tag{87}$$

where $B(a,b) = \int_0^1 t^{a-1}(1-t)^{b-1}dt$ is the beta function and $I_p(a,b) = \int_p^1 t^{a-1}(1-t)^{b-1}dt/B(a,b)$ is the incomplete beta function. The critical cluster size $k(\sigma)$ is

$$k(\sigma) \approx \left\{ \left(\frac{\sigma}{a\sigma_\delta}\right)^{-\frac{\rho}{2\beta_1}} - \frac{b\rho}{4\beta_1} + \frac{b^2\rho\gamma}{8\beta_1^2} \left(\frac{\sigma}{a\sigma_\delta}\right)^{\frac{\rho}{2\beta_1}} \right\}^2. \tag{88}$$

Figure 15 shows $W_\infty(\sigma)$ from Eq. (85) together with the $\hat{W}(\sigma)$ distributions obtained through Monte Carlo simulation, assuming the power-law distribution $F_p(\sigma)$ for fiber strength. For all three sizes shown, the theoretical and empirical distributions agree even at $\rho = 1$, whereas in

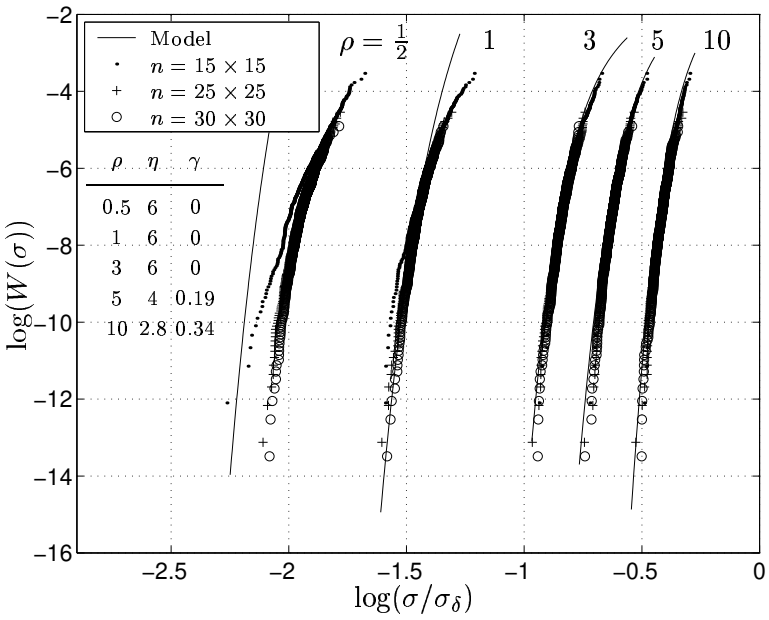

Figure 15. Comparison of the characteristic distribution function $W(\sigma)$ from the cluster growth model under 2D HVLLS and power-law fiber strength $F_p(\sigma)$ with the empirical version $\hat{W}(\sigma)$ obtained from Monte-Carlo simulations. The values of (η, γ) used here are identical to those in Figure 13 for Model 2.

Figure 13 assuming Weibull fibers they began to diverge at $\rho = 2$. Apparently, as ρ decreases in the Weibull case, the stalling probability of a growing cluster is increased by occasional strong fibers thus promoting dispersed breaking, but this does not occur under the power-law version of $F_p(\sigma)$, which has no fibers with strength exceeding σ_δ. Surprisingly, even at $\rho = 0.5$, reasonable agreement of the cluster growth model with the simulations occurs under $F_p(\sigma)$.

5. Analysis of Composite Strength Distribution for Small ρ

In the case of dispersed fiber failure in a δ-bundle, it is reasonable to conjecture that for small enough ρ the details of the fiber load-sharing model are not important provided that the model conserves load. Thus we consider behavior under the equal load-sharing rule, or ELS, where the stress concentration factor for each intact fiber in an n-fiber δ-bundle with j broken fibers is $\kappa_{n,j} = n/(n-j)$, as described in Section 1.2. Daniels (1945) showed that if the strengths of individual fibers are independent and identically distributed according to an

arbitrary distribution function $B(\sigma)$, and certain conditions are met such as $\lim_{\sigma\uparrow\infty}\sigma(1-B(\sigma))=0$ and the peak in the maximum of this function is unique, then the strength distribution $G_n(\sigma)$ of a δ-bundle asymptotically converges, as $n\to\infty$, to the normal or Gaussian form $\Phi((\sigma-\mu_n^*)/s_n^*)$ where

$$\mu_n^* = \mu^* = \sigma_\tau(1-B(\sigma_\tau)), \tag{89}$$

and

$$s_n^* = \sigma_\tau n^{-1/2}\sqrt{nB(\sigma_\tau)(1-B(\sigma_\tau))}, \tag{90}$$

and where σ_τ gives $\sigma(1-B(\sigma))$ its maximum value. Here $\Phi(\cdot)$ denotes the standard Gaussian distribution.

$$\Phi(z) = \frac{1}{\sqrt{2\pi}}\int_{-\infty}^{z} e^{-u^2/2}du. \tag{91}$$

As mentioned in Section 1.4, Smith (1982) gave a correction to the asymptotic mean to speed up convergence to the asymptotic limit. Applying Daniels' formula with Smith's correction to the Weibull fiber case, one obtains a very accurate prediction of the true strength distribution, even for quite small n. The parameters of the resulting normal strength distribution are then the asymptotic mean

$$\mu_n^* = \sigma_\delta(\rho e)^{-1/\rho}\left\{1+0.996n^{-2/3}\left(e^{2/\rho}/\rho\right)^{1/3}\right\}, \tag{92}$$

and the asymptotic standard deviation

$$s_n^* = \sigma_\delta n^{-1/2}\rho^{-1/\rho}\sqrt{e^{-1/\rho}(1-e^{-1/\rho})}. \tag{93}$$

In Subsection 3.2 we observed from Monte Carlo simulations that, when $\rho\downarrow 0$ and the variability in fiber strength increases, the δ-bundle strength distributions under both HLLS and HVLLS converge to the Gaussian or normal form of ELS, for the bundle sizes n considered. Two reasons were cited: The first was the tendency for small clusters to stall from the dominance of strong fibers from the Weibull upper tail, and the second was increasing numbers of very weak fibers causing many more scattered clusters. The question arises as to whether this behavior persists as n increases by orders of magnitude.

We conjecture that, no matter how small the value of ρ and no matter how much initial dispersed fiber failure, if a δ-bundle is large enough final failure will eventually be locally initiated and a cluster will eventually propagate catastrophically to fail the rest of the surviving fibers. That is, unlike ELS, wherein material damage truly accrues globally, we conjecture that in HLLS and HVLLS there is a ρ-dependent

size scale within which damage initiates and propagates. This must remain a conjecture because we are unable to simulate δ-bundles much beyond $n = 900$, yet under 2D HVLLS and $\rho = 0.5$ the critical cluster size is probably greater than 900 fibers. Nevertheless evidence for this assertion is seen from simulations on large 1D HLLS δ-bundles.

For 1D HLLS, Figure 16 shows the evolution of fiber breaks that occur in the median strength (out of $N = 500$) δ-bundle with $n = 900$ fibers and for $\rho = 0.5$, 1, and 10. For $\rho = 0.5$ a cluster does not initiate, as the fiber failures are largely dispersed to the very end. This happens even though the bundle size $n = 900$ is much larger than the critical cluster size. The final load increment occurs when 90% of the fibers have already failed. For $\rho = 1$, however, although breaks are initially dispersed up to the failure of slightly less than half of the fibers, the remaining fibers fail as a sharply growing cluster. For $\rho = 10$ there are just a few initial dispersed breaks, but then a sharply growing, catastrophic cluster develops near fiber number 600.

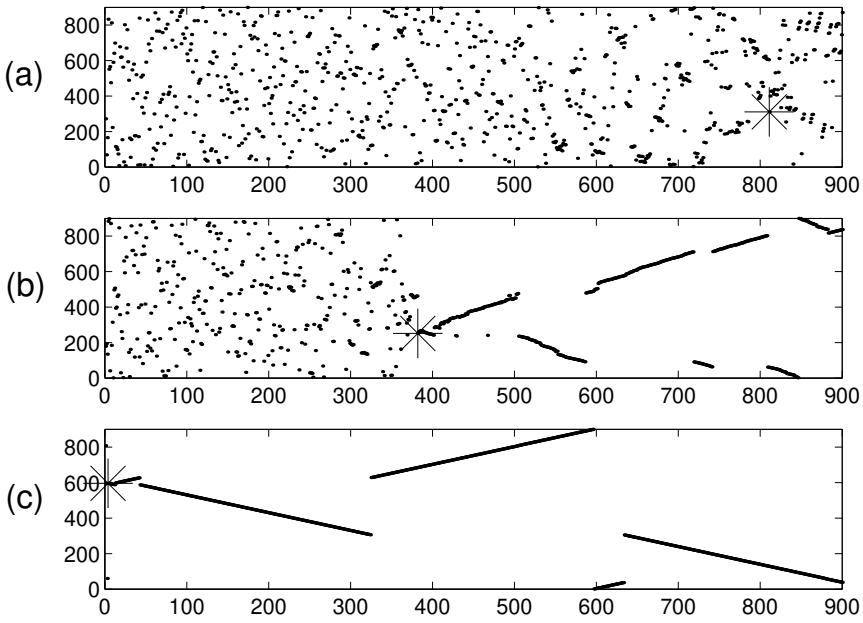

Figure 16. Fiber break sequence in median strength (among 500 simulations) 900-fiber δ-bundles under 1D HLLS with (a) $\rho = 0.5$, (b) $\rho = 1$ and (c) $\rho = 10$. A dot is plotted at coordinates (N_x, N_y) if fiber number N_y is the N_x-th to fail. The first fiber to fail with the last load increment is labeled $*$. The strengths of these specimen are 0.5089 for the $\rho = 0.5$ specimen, 0.3075 for $\rho = 1$, and 0.5964 for $\rho = 10$.

For $\rho = 1/2$, Figure 17 shows the break evolution sequence for the weakest and median among $N = 100$ δ-bundles with $n = 1500$ fibers. The weakest specimen develops a cascading cluster after about two-thirds of the fibers have failed. However, it develops considerable dispersion at the cluster edge and eventually stalls. Further load increments lead to additional dispersed failures followed by a final cascading cluster from a new location when only one-tenth of the fibers remain. The median 1500 fiber specimen, however, initiates cluster growth after about four-fifths of the fibers have failed and this cluster propagates without stalling until the composite fails.

Comparing with Figure 16, the conclusion from Figure 17 is that for small ρ the cluster growth mode may not dominate until the δ-bundle reaches a certain large size well beyond the critical cluster size. Even then the network is drastically diluted by the dispersed failure mode. As it weakens with increasing size, however, we conjecture that the cluster growth mode will increasingly dominate, at least in 1D HLLS bundles.

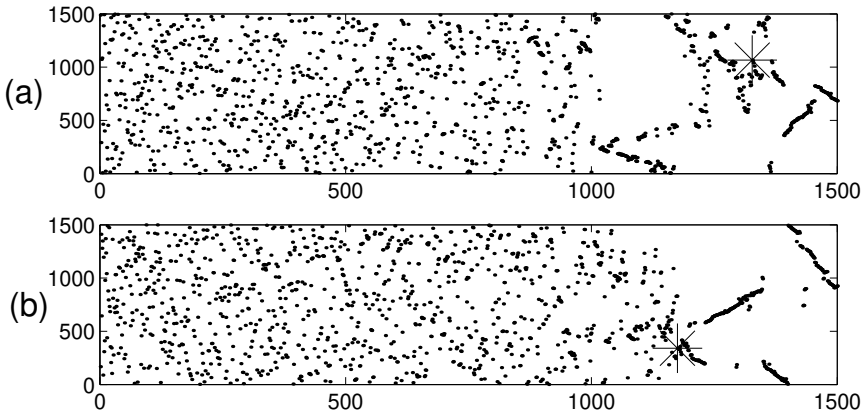

Figure 17. Fiber break sequence in a 1500 fiber δ-bundle under HLLS for $\rho = 0.5$: (a) weakest (lower tail) and (b) median specimen among 100 simulations. The strength of the weakest specimen is 0.3872 and of the median specimen is 0.5053. The first fiber to break with the last load increment is labeled $*$.

Although clusters may eventually form, there remains considerable dispersion and diluting of the number of intact fibers under ELS-like behavior. Thus the localized nature of the load-sharing rule is finally superimposed onto a diluted set of fibers following ELS failure statistics. One possibility for the breakdown mechanism is that local patches begin to break down following the statistics of a scale limited version of ELS, and if a patch is beyond critical size it propagates catastrophically. The statistics of the weakest ELS-like patch determines the strength

distribution of the δ-bundle. A second possibility is that broad dilution of the number of surviving fibers occurs due to ELS-like behavior and local cluster growth eventually develops under a revised local load sharing mechanism on the randomly diluted set of survivors. Along these lines a 1D model under a tapered local load-sharing rule was recently developed by Phoenix and Beyerlein (2000b) where a weakest-link model with a characteristic distribution function $W(\sigma)$ was derived of the form given by Eq. (40) for 1D HLLS. In their work a nontrivial exponent arose from the local combinatorics of the dilution playing a role similar to the values of (η, γ) in Figures 13 and 15.

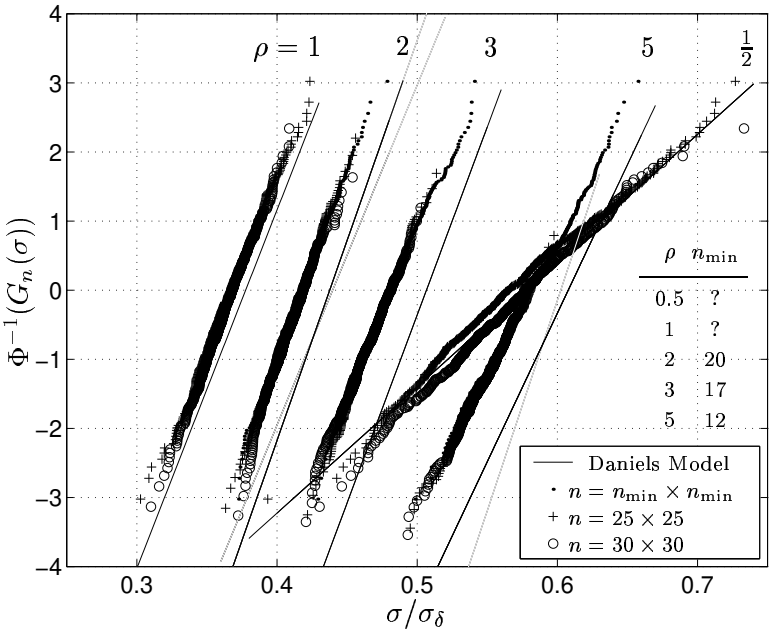

Figure 18. Comparison of $\Phi((\sigma - \mu_n^*)/s_n^*)$ given by Daniels' formula for ELS δ-bundles, Eq. (95), with weak-linked strength distributions obtained from simulations. Strength distributions for sizes $n = 625$ and 900 are weak-linked to size $n_{\min}^2$ as listed in the figure. For $\rho = 2$, 3, and 5, the distributions of $n = 625$ and 900 δ-bundles when weak-linked to size $n_{\min}^2$ appear to collapse into the strength distribution of a δ-bundle with $n_{\min}^2$ fibers chosen to be the smallest with this property. For $\rho = 0.5$ and 1 no such collapse is observed. For $\rho = 0.5$ the agreement of the strength distribution of the $n = 625$ δ-bundle and the $n = 900$ δ-bundle weak-linked to size 625 is spurious. Such agreement is not observed for a 2500 fiber δ-bundle weak-linked to size 625.

A model consistent with the first scenario is that failure initiates following an ELS-like failure mechanism in a patch of $\tilde{n}$ fibers smaller than n when sufficiently large. The strength of this patch has Gaussian

character, and δ-bundle failure corresponds to the failure of the weakest of the $\tilde{m} = n/\tilde{n}$, $\tilde{n}$-fiber patches. That is,

$$G_n(\sigma) = 1 - \{1 - \Phi[(\sigma - \mu^*_{\tilde{n}})/s^*_{\tilde{n}})]\}^{\tilde{m}}, \tag{94}$$

where $\Phi(\cdot)$ denotes the standard normal distribution and $\mu^*_{\tilde{n}}$ and $\sigma^*_{\tilde{n}}$ are defined in Eqs. (92) and (93). For small σ, we may replace $\Phi(\cdot)$ with

$$\tilde{\Phi}(z) = \frac{1}{\sqrt{2\pi}\ |z|} \exp(-z^2/2), \tag{95}$$

which is the asymptotic form of the lower tail of the standard normal distribution. Likewise, that for the composite, $H_{m,n}(\sigma)$, is simply the above result with $\tilde{m}$ replaced by $m\tilde{m}$. Use of this result in other composite settings is found in Phoenix et al. (1997). The parameters of the Gaussian weakest-link distribution are given by the Smith corrected, Daniels formula Eq. (92) and (93).

In Figure 18, for $\rho = 1$, 2, 3, and 5 we have plotted the strength distribution of the smallest sized δ-bundle ($n_1 \times n_1$) to which weak-link scaled distributions for larger bundles collapse. This minimum δ-bundle size approximately corresponds to the critical cluster size defined previously. We also show the distributions of larger bundles of size ($n_2 \times n_2$) or ($n_3 \times n_3$) weak-linked to the size ($n_1 \times n_1$). Note that as ρ is decreased, the weak-linked distributions become increasingly Gaussian (indicated by the straightness of the strength distribution on normal coordinates) and are better approximated by the ELS asymptotic distribution, though a shift exists for $\rho \geq 1$.

In the case $\rho = 0.5$, despite the excellent agreement of the 900-fiber, weak-linked strength distribution with the 625-fiber, weak-linked distribution, it turns out that they do not agree with a 2500-fiber, weak-linked δ-bundle strength distribution (of which limited results were generated but are not shown). This suggests that the smallest catastrophic failure event of the bundle occurs over more than 625 or perhaps even 900 fibers. The same may also hold in the $\rho = 1$ case. However, for $\rho \geq 2$, the maximum simulation cell size of $n = 30 \times 30$ seems to be adequate to contain the catastrophic failure event.

In the cases $\rho \leq 1$ it is unclear if the upper-tail, strong fiber dominance will continue for much larger bundles (with smaller strengths). Unfortunately, simulating such bundles is presently computationally infeasible. If it is so that the weakest link involves strong fibers and ELS dispersed failure over limited scale, Eq. (94) will hold for the δ-bundle strength distribution. If not, the weakest link mechanism will revert to the cluster growth model, though with dispersed fiber breaking ahead of the cluster tip, and Eq. (73) may hold when modified to account for the extensive dilution by fiber breaks.

6. Analysis of Effect of ρ on Statistical Failure Mode

We have seen that δ-bundle failure for both 1D HLLS and 2D HVLLS shows a transition from a break cluster growth mode to a dispersed fiber failure mode somewhere in the neighborhood of $\rho = 1$ to 2. We now investigate certain statistical aspects of cluster growth that may suggest the potential for such a transition. While the stress concentrations on the neighbors of an r-cluster increase their probabilities of failure, the extent appears to depend on ρ thus influencing the onset of instability.

6.1. Effect of ρ on Tendency for Cluster Stalling

To investigate the effect of decreasing ρ on r-cluster growth, we add one break to form an $(r+1)$-cluster and let $\Delta(r, n')$ be the mean number of additional fibers among its n' nearest intact neighbors that will fail due to the increased load from the break, assuming all fibers have survived the previous load. We let the applied fiber stress σ be small enough that the fiber failure probability $F(K_r\sigma)$ from Eq. (1) is well approximated by $F(K_r\sigma) \approx (K_r\sigma/\sigma_\delta)^\rho$ in the case of Weibull fibers and is exact in the case of power-law fibers. Then,

$$\Delta(r, n') \approx n'(K_{r+1}^\rho - K_r^\rho)\,(\sigma/\sigma_\delta)^\rho\,. \tag{96}$$

Since $K_{r+1} > K_r > 1$, we see that $K_{r+1}^\rho - K_r^\rho$ is an increasing function of ρ so that for fixed n' and σ, $\Delta(r, n')$ increases with ρ. Thus, when ρ is small the addition of a fiber break to an r-cluster causes fewer neighbors to fail due to overloads.

We may specialize Eq. (96) to the case of a penny-shaped r-cluster in a 2D planar fracture surface. In this case, $n' = 2\sqrt{\pi r}$ and we get using Eq. (16)

$$\begin{aligned}\Delta(r, 2\sqrt{\pi r}) &\approx 2\sqrt{\pi r}\left\{\left(1 + \frac{2\sqrt{r+1}}{\pi^{3/2}}\right)^{\rho/2} - \left(1 + \frac{2\sqrt{r}}{\pi^{3/2}}\right)^{\rho/2}\right\}\left(\frac{\sigma}{\sigma_\delta}\right)^\rho, \\ &\approx C_\rho r^{\frac{\rho}{4}-\frac{1}{2}}\left(\frac{\sigma}{\sigma_\delta}\right)^\rho \quad \text{for large } r.\end{aligned} \tag{97}$$

Thus the number of breaks around a large cluster tends to increases with r for $\rho > 2$ but decreases with r for $\rho < 2$ where the cluster will tend to stall.

This argument, however, does not account for the fact that the addition of a single break at the cluster edge will expose a few fibers in its vicinity to a much larger jump in stress of the order of from $(1/2)K_r\sigma/\sigma_\delta$ to $K_{r+1}\sigma/\sigma_\delta$, and the associated probability of failure

for each of these is of order $(K_{r+1}\sigma/\sigma_\delta)^\rho$, which does not show this transition to an expected decrease as ρ decreases. This aspect of the problem may explain the need for Eq. (50), and the values of N_r based on the values η and γ given in Figures 13 and 15 seem reasonable in this light.

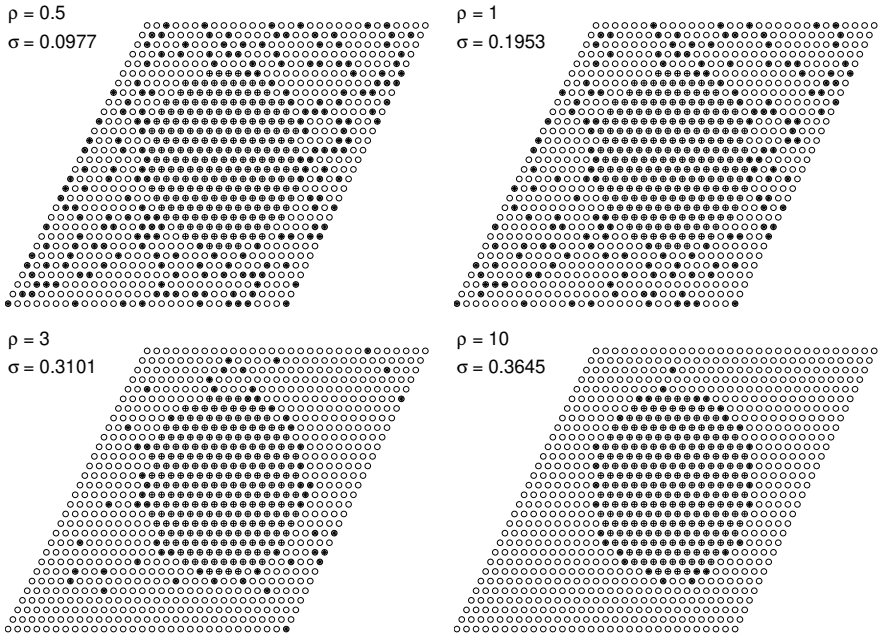

Figure 19. Transition from dispersed fiber failure to cluster enlargement around an initial, tight 239-break cluster, which occurs as ρ increases.

6.2. Effect of ρ on Break Dispersion Near Cluster Edge

Another important aspect to consider as ρ decreases is the location of new breaks due to an r-cluster introduced into a δ-bundle. Figure 19 shows a simulation of the fiber failures that immediately occur due to the presence of a penny-shaped cluster of $r = 239$ breaks introduced into a 2D δ-bundle under the numerical version HVLLS. In each of the four cases, the fiber strengths were derived from the same set of uniformly distributed random numbers U_i, so the Weibull strength of the j-th fiber in each case is $(-\log(U_j))^{1/\rho}$. The applied stress σ was chosen in each of the four cases so that the probability of failure of a fiber adjacent to the cluster edge was about 1/2, i.e., $(K_{239}\sigma/\sigma_\delta)^\rho \approx 0.69$, where $K_{239} = 2.56$ from Eq. (16). These breaks would typically cause even more breaks without a change in applied load, but these

secondary breaks are not shown. Observe that for the same approximate number of fiber failures in the ring around the cluster, serving to extend it, an increasing number of fibers fail away from the cluster as ρ is decreased. Many of the ones appearing for $\rho = 1/2, 1$ and 3 would have occurred anyway under the applied stress σ/σ_δ with probability $F(\sigma)$ given by Eq. (1). Nevertheless, as ρ decreases, dispersive effects at the edge begin to appear.

To understand these dispersive effects, we may evaluate the probability of failure of a fiber at distance s away from an r-cluster. Its probability of failure is $(K_{r,s}\sigma/\sigma_\delta)^\rho$ or, using Eq. (17),

$$\Pr\{\text{fiber failure at distance } s\} = \left(\frac{1}{1+\pi(s-1)}\right)^{\rho/2} \left(\frac{K_r\sigma}{\sigma_\delta}\right)^\rho. \quad (98)$$

This result holds approximately for $1 \le s \le \epsilon D$ where ϵ is about $1/10$, and $D = 2\sqrt{r/\pi}$ is the cluster diameter. This is roughly the range of influence of the cluster "tip" (analogous to the K-field in linear elastic fracture mechanics). Clearly the first factor in Eq. (98) increases with decreasing ρ and leads to an increased number of fiber failures away from the cluster edge as compared to fibers right at the edge ($s = 1$). Beyond this range the stress is close to the far field value, σ. In the present case $r = 239$, $D \approx 18$, and the range is $1 \le s \le 2$ covering just two fibers from the edge. Nevertheless one can see increasing numbers of breaks near the edge in the sub-adjacent neighbors as ρ decreases.

We can use Eq. (98) to illustrate a more subtle aspect of the effect of ρ as suggested in Figure 19. Suppose that as ρ is decreased, the applied stress σ is chosen such that $(K_r\sigma/\sigma_\delta)^\rho = C \ll 1$, where C is independent of ρ. We may estimate the number of fibers that immediately fail due to the introduction of the penny-shaped r-cluster where r is large. This requires evaluating the integral

$$\left(\frac{K_r\sigma}{\sigma_\delta}\right)^\rho \int_1^{\epsilon 2\sqrt{r/\pi}} \frac{2\pi(s+\sqrt{r/\pi})}{(1+\pi(s-1))^{\rho/2}} ds,$$

where $2\pi(s+\sqrt{r/\pi})$ is the number of fibers in a ring of radius $s+\sqrt{r/\pi}$ outside the cluster and the rest of the integrand is the probability of a fiber failure in that ring. Upon evaluating the integral we notice that the result asymptotically has the factor $r^{1-\rho/4}$. Thus as r increases this integral behaves differently for $\rho > 4$ versus $\rho \le 4$, converging in the former case and diverging in the latter. This suggests that as ρ decreases below 4, in the vicinity of a large 2D break cluster under HVLLS, new breaks are more likely away from the cluster than around its edge. Repeating this calculation for a 1D cluster of r breaks under HLLS, one finds that $\rho = 2$ is the transition value for divergence.

On the other hand, as a δ-bundle fails when σ is increased, intact fibers will typically have survived previous stress levels. Thus a variant of the above calculation is to assume that all fibers have been "proof-tested" just enough to support stress σ on the δ-bundle *with* the penny-shaped r-cluster, and that a small stress increment $\Delta\sigma$ is required to induce failures. It can be shown that ρ effectively is replaced by $\rho - 1$ in the result so the threshold for divergence increases to $\rho = 5$ in 2D HVLLS and $\rho = 3$ in 1D HLLS.

Suemasu (1982) conducted an investigation somewhat like the one above, except that he concentrated on the stress transferred from only one break to other fibers over the whole composite. In the plane of the break this overload scales as s^{-2} in the 1D HLLS case and s^{-3} in 2D HVLLS. To this he added the applied stress σ, which the fibers were assumed to have previously survived. Because he integrated the decaying overload along fibers (far outside our δ-bundles) he concluded for all $\rho > 0$ that divergence occurs in the number of flaws broken in all fibers over the whole composite due to one break. However, repeating his calculation over fibers within a δ-bundle leads to convergence for all $\rho > 0$, so little insight into the role of ρ is gained without focusing on large clusters with $1/\sqrt{s}$ fiber stress decay at their edges.

These arguments indicate that during δ-bundle failure under increasing σ, the tendency towards dispersed fiber failures versus cluster growth increases as ρ decreases, but the values of ρ determined above are too high to directly explain the transition. Also, when ρ is small, the probability of finding very weak fibers below strength σ is much more than when ρ is large, and thus many dispersed fiber breaks are to be expected. This aspect appears to be borne out by Figures 3 and 7, and Figure 19 as well as by inspection of many simulations.

In addition to ρ, the number of fibers n in the δ-bundle also plays a role in the occurrence of a dispersed versus a cluster growth failure mode. Smaller composites tend to be stronger, and thus, show a higher proportion of dispersed fiber breaks caused by the applied stress σ. Also, clusters are smaller when they become unstable. In larger composites, the cluster size required for instability is larger, mainly because the applied stress σ is smaller (i.e., the composite is weaker) and a higher stress concentration at the cluster edge is needed to fail fibers. Nevertheless, it appears that no matter how large the cluster is before instability, the tendency when ρ is small is to form dispersed breaks at the cluster edge as it grows, thus spreading the stress redistribution.

7. Conclusions and Relations to Other Results

In Eqs. (40) and (73) we have the weakest-link, characteristic distribution function $W(\sigma)$ for 1D and 2D δ-bundles under HLLS and HVLLS, respectively. These bundles are links in the chain-of-bundles model for the failure of large 2D and 3D unidirectional composites, respectively. For sufficiently large Weibull modulus ρ, say $\rho > 2$ in 3D composites and $\rho > 1$ in 2D planar composites, the strength distribution of a composite of length $L = m\delta$ and with n fibers is $H_{m,n}(\sigma) \approx 1 - (1 - W(\sigma))^{mn}$. When ρ decreases below these values, however, the details of the load-sharing become increasingly unimportant, and the δ-bundle strength distribution for fixed n is not only increasingly Gaussian up to quite large n but also converges to that for ELS whose analytical form was given. For fixed ρ, however, this Gaussian nature is expected to persist only up to a δ-bundle size of the order of the critical cluster size increased to eliminate the likelihood of stalling. Then the distribution function for δ-bundle strength appears to be that for a chain of Gaussian 'patches' of $\tilde{n}$ fibers in the δ-bundle, particularly under 2D HVLLS. Thus the composite can be viewed as a weakest-link arrangement of $m\tilde{m}$ such Gaussian patches. As the number of fibers n in the composite increases by orders of magnitude, it is not clear that this Gaussian nature will persist, especially in 1D HLLS.

Simpler versions of the form for $W(\sigma)$, Eq. (40), have been derived in related failure models where elements have strength 0 or 1 with probability p and $1 - p$, respectively. See for example Duxbury and Leath (1987), Harlow and Phoenix (1991) and Phoenix and Beyerlein (2000b), where in the latter two works power prefactors were obtained in $W(\sigma)$ as here. Very recent work, carried out by Wu and Leath (2000a; 2000b) under similar assumptions, has yielded distribution forms very similar to those here. Earlier versions are also given in Phoenix and Beyerlein (2000a). In the time dependent setting, analogous versions, $W(t)$, have been obtained without a power prefactor by Curtin and Scher (1997) and Curtin et al. (1997), and with a power factor by Newman and Phoenix (2001). In these works hard transitions to Gaussian lifetime behavior were noted when a breakdown parameter decreased below a certain critical value.

Fiber break clusters need not lie in a transverse plane but can wander out of plane since new breaks can form next to old ones anywhere within length δ. However the tendency towards alignment is fairly strong unless the variability in fiber strength is large. Nevertheless, the idea of using a single length-scale δ for fiber load transfer may be unrealistic when large break clusters develop before instability. Thus the chain-of-bundles concept may be too restrictive in certain cases

and the load-sharing model may require revision beyond using the fiber load values obtained along a single break plane.

To account for some of these features, simulation results have been generated by Landis et al. (2000) for a true 3D model using a modified, square array version of HVLLS with eight matrix shear couplings rather than four. Their results were successfully modeled by Phoenix and Beyerlein (2000a) using the Gaussian-link approach of the dispersed failure mode at the end of the last section, but generalized to elastic global load-sharing. Using the $W(\sigma)$ cluster growth approach here Phoenix and Beyerlein (2000a) were only able to model quite well their results for $\rho = 20$ but not $\rho = 10$ and 5 where misfits similar to those appearing in Figure 13 occurred. As here, using Eq. (50) for N_r and adjusting γ and η may greatly improve the fit, but nevertheless, the range for ρ corresponding to a dispersed failure mode may have a higher transition value than observed here.

We also mention work by Ibnabdeljalil and Curtin (1997) for a lattice-based model similar to HVLLS but with the added features of fiber slip and pullout at breaks causing tractions across the final fracture plane. Their Monte Carlo simulation results for $\rho = 5$ and 10 were successfully modeled using the Gaussian-link approach of the dispersed failure mode described at the end of the previous section, but generalized to global load-sharing as in Curtin (1991) and Phoenix et al. (1997)). Using a version of the cluster growth model here, which assumes $\gamma = 1/2$ in $W(\sigma)$, Phoenix and Beyerlein (2000a) were able to model fairly well their results for $\rho = 10$ but not $\rho = 5$ where misfits occurred similar to those appearing in Figure 13. Again, using Eq. (50) and adjusting γ and η may greatly improve the fit but once more the transition ρ value for a dispersed failure mode may be higher than observed here. In practice there may actually be considerable overlap in the ranges for ρ where the two models may apply.

We have set the length of a δ-bundle to be δ of Eq. (9). In reality this definition tends to produce too large a composite failure probability in the chain-of-bundles model because of the stress decay along a fiber from its peak in actual composites. This reduces the probability of finding a flaw. A more realistic definition of δ involves ρ (or one can modify the definition of K_r also involving ρ) as discussed in Phoenix and Beyerlein (2000a). Except for a shift in stress scale and change in the value of m, revising the definition of δ has negligible effect on our results. Although we use the same characteristic length scale, δ, in HLLS and HVLLS, the physical decay length along a fiber is about one-half that in the HLLS case for the same volume fraction of fiber since there are three times as many fiber-to-fiber couplings in HVLLS.

Acknowledgements

SLP acknowledges financial support from the National Science Foundation (CMS-9800413) and from the National Institute of Standards and Technology (PO#43SBN867130). IJB gratefully acknowledges support by the Department of Energy office of Basic Energy Sciences and the Structure/Property Relations group at Los Alamos National Laboratory. SM acknowledges generous support under a GRA while doing the bulk of the work at Los Alamos National Laboratory.

References

Argon, A.S. (1974). Statistical Aspects of Fracture. *in Fracture and Fatigue, L. J. Broutman, ed., Academic Press, New York*, pp. 153–190

Batdorf, S.B. (1982). Tensile strength of unidirectionally reinforced composites. *International Journal Reinforced Plastics and Composites* **1**, pp. 153–164.

Batdorf, S.B. and Ghaffarian, R. (1982). Tensile strength of unidirectionally reinforced composites II. *International Journal of Reinforced Plastics and Composites* **1**, pp. 165–176.

Beyerlein, I.J. and Phoenix, S.L. (1997a). Statistics of fracture for an elastic notched composite lamina containing Weibull fibres – Part I. Features from Monte-Carlo simulations. *Engineering Fracture Mechanics* **57**, pp. 241–265.

Beyerlein, I.J. and Phoenix, S.L. (1997b). Statistics of fracture for an elastic notched composite lamina containing Weibull fibres – Part II. Probability models of crack growth. *Engineering Fracture Mechanics* **57**, pp. 267–299.

Beyerlein, I.J., Phoenix, S.L., and Sastry, A.M. (1996). Comparison of shear-lag theory and continuum fracture mechanics for modeling fiber and matrix stresses in an elastic cracked composite lamina. *International Journal of Solids and Structures* **33**, pp. 2543–2574.

Coleman, B.D. (1958). On the strength of classical fibres and fibre bundles. *Journal of the Mechanics Physics of Solids* **7**, pp. 60–70.

Curtin, W.A. (1991). Theory of mechanical properties of ceramic matrix composites. *Journal of the American Ceramic Society* **74**, pp. 2837–2845.

Curtin, W.A. (1999). Stochastic damage evolution and failure in fiber-reinforced composites. *Advances in Applied Mechanics* **36**, pp. 163–253.

Curtin, W.A. and Scher, H. (1997). Time-dependent damage evolution and failure in materials. I. Theory. *Physical Review B* **55**, pp. 12038-12050.

Curtin, W.A., Pamel, W., and Scher, H. (1997). Time-dependent damage evolution and failure in materials. II. Simulations. *Physical Review B* **55**, pp. 12051–12061.

Daniels, H.E. (1945). The statistical theory of the strength of bundles of threads I *Proceedings of the Royal Society. London A* **183**, pp. 405–435.

Duxbury, P.M. and Leath, P.L (1987). The failure distribution in percolation models of breakdown. *Journal of Physics A: Mathematical and General* **20**, pp. L411–L415.

Goda, K. and Phoenix, S. L. (1994). Reliability approach to the tensile strength of unidirectional CFRP composites by Monte-Carlo simulation in a shear-lag model. *Composite Science and Technology* **50**, pp. 457–468.

Goda, K. (1999). The role of interfacial debonding in increasing the strength and reliability of unidirectional fibrous composites. *Composite Science and Technology* **59**, pp. 1871–1879.

Gücer D.E. and Gurland, J. (1962). Comparison of the statistics of two fracture modes. *Journal of the Mechanics Physics of Solids* **10**, pp. 365–373.

Harlow, D.G. and Phoenix, S.L. (1978a). The chain-of-bundles probability model for the strength of fibrous materials I : analysis and conjectures. *Journal of Composite Materials* **12**, pp. 195–214.

Harlow, D.G. and Phoenix, S.L. (1978b). The chain-of-bundles probability model for the strength of fibrous materials II: a numerical study of convergence. *Journal of Composite Materials* **12**, pp. 314–334.

Harlow, D.G. and Phoenix, S.L. (1981). Probability distributions for the strength of composite materials II: a convergent sequence of tight bounds. *International Journal of Fracture* **17**, pp. 60l–630.

Harlow, D.G. and Phoenix, S.L. (1991). Approximations for the strength distribution and size effect in an idealized lattice model of material breakdown. *Journal of the Mechanics and Physics of Solids* **39**, pp. 173–200.

Hedgepeth, J.M. (1961). Stress concentrations in filamentary structures. *NASA TND–882*.

Hedgepeth, J.M. and Van Dyke, P. (1967). Local stress concentrations in imperfect filament composites. *Journal of Composite Materials* **1**, pp. 294–309.

Hikami, F. and Chou, T.W. (1990). Explicit crack problem solutions of unidirectional composites: Elastic stress concentrations. *AIAA Journal* **22**, pp. 499–505.

Ibnabdeljalil, M. and Curtin, W.A. (1997). Strength and reliability of fiber reinforced composites: Localized load-sharing and associated size effects. *International Journal of Solids and Structures* **34**, pp. 2649–2668.

Kuo, C.C. and Phoenix, S.L. (1987). Recursions and limit theorems for the strength and lifetime distributions of a fibrous composite. *Journal of Applied Probability* **24**, pp. 137–159.

Landis, C.M., Beyerlein, I.J. and McMeeking, R.M. (2000). Micromechanical simulation of the failure of fiber reinforced composites. *Journal of the Mechanics and Physics of Solids* **48**, pp. 621–648.

Leath, P.L. and Duxbury, P.M. (1994). Fracture of heterogeneous materials with continuous distributions of local breaking strengths. *Physical Review B* **49**, pp. 14905–14917.

Mahesh, S., Beyerlein, I.J. and Phoenix, S.L. (1999). Size and heterogeneity effects on the strength of fiber composites. *Physica D* **133**, pp. 371–389.

Manders, P.W., Bader, M.G. and Chou, T.-W. (1982). Monte Carlo simulation of the strength of composite fibre bundles. *Fibre Science and Technology* **17**, pp. 183–204.

McCartney, L.N. and Smith, R.L. (1983). Statistical theory of the strength of fiber bundles. *ASME Journal of Applied Mechanics* **105**, pp. 601–608.

Newman, W.I. and Phoenix, S.L. (2001). Time-dependent fiber bundles with local load sharing. *Physical Review E* **63**, pp. 021507-1–20.

Phoenix, S.L., and Beyerlein, I.J. (2000a). Statistical Strength Theory for Fibrous Composite Materials, *Chapter 1.19 in Vol. 1 (T.-W. Chou, ed.) of Comprehensive Composite Materials (A. Kelly and C. Zweben, series eds.), Pergamon - Elsevier Science*, pp. 559–639.

Phoenix, S.L., and Beyerlein, I.J. (2000b). Distributions and size scalings for strength in a one-dimensional random lattice with load redistribution to nearest and next-nearest neighbors. *Physical Review E* **62**, pp. 1622–1645.

Phoenix, S.L., Ibnabdeljalil, M. and Hui, C.-Y. (1997). Size effects in the distribution for strength of brittle matrix fibrous composites. *International Journal of Solids and Structures* **34**, pp. 545–568.

Phoenix, S.L. and Smith, R.L. (1983). A comparison of probabilistic techniques for the strength of fibrous materials under local load-sharing among fibers. *International Journal of Solids and Structures* **19**, pp. 479–496.

Rosen, B.W. (1964). Tensile failure of fibrous composites. *AIAA Journal* **2**, pp. 1985–1991.

Scop, P.M. and Argon, A.S. (1967). Statistical theory of strength laminated composites. *Journal of Composite Materials* **1**, pp. 92–99.

Scop, P.M. and Argon, A.S. (1969). Statistical theory of strength laminated composites II. *Journal of Composite Materials* **3**, pp. 30–47.

Smith, R.L. (1980). A probability model for fibrous composites. *Proceedings of the Royal Society, London A* **372**, pp. 539–553.

Smith, R.L. (1982). The asymptotic distribution of the strength of a series-parallel system with equal load sharing. *Annals of Probability* **10**, pp. 137–171.

Smith, R.L. (1983). Limit theorems and approximations for the reliability of load-sharing systems. *Advances in Applied Probability* **15**, pp. 304–330.

Smith, R.L., Phoenix, S.L., Greenfield, M.R., Henstenburg, R.B. and Pitt, R.E. (1983). Lower-tail approximation for the probability of failure of three-dimensional fibrous composites with hexagonal geometry. *Proceedings of the Royal Society, London A* **388**, pp. 353–391.

Suemasu, H. (1982). An analytical study of probabilistic aspects of strength of unidirectional fiber reinforced composites under tensile loads. *Transactions of the Japanese Society for Composite Materials* **8**, pp. 29–36.

Wu, B.Q., and Leath, P.L. (2000a). Fracture strength of one-dimensional systems with continuous disorder: a single-crack approximation. *Physical Review B* **61**, pp. 15028–15034.

Wu, B.Q., and Leath, P.L. (2000b). Similarity of growing cracks in breakdown of heterogeneous planar interfaces. *Physical Review B* **62 no. 13**.

Zhang, S.D., and Ding, E.J. (1996). Failure of fiber-bundles with local load-sharing. *Physical Review B* **53**, pp. 646–654.

Zweben, C. (1968). Tensile failure of fiber composites. *AIAA Journal* **6**, pp. 2325–2331.

Zweben, C. and Rosen, B.W. (1970). A statistical theory of material strength with application to composite materials. *Journal of the Mechanics and Physics of Solids* **18**, pp. 189–206.